CD103+CD8+ TRM Cells Accumulate in Tumors of Anti-PD-1-Responder Lung Cancer Patients and Are Tumor-Reactive Lymphocytes Enriched with Tc17

Stéphanie Corgnac, Ines Malenica, Laura Mezquita, Edouard Auclin, Elodie Voilin, Jamila Kacher, Heloise Halse, Laetitia Grynszpan, Nicolas Signolle, Thibault Dayris, et al.

CD103^{+}CD8^{+} T_{RM} cells accumulate in tumors of anti-PD-1-responder lung cancer patients and are tumor-reactive lymphocytes enriched with Tc17

Stéphanie Corgnac[1], Ines Malenica[1], Laura Mezquita[2*&], Edouard Auclin[3*], Elodie Voilin[1], Jamila Kacher[1], Heloise Halse[1], Laetitia Grynszpan[1], Nicolas Signolle[4], Thibault Dayris[5], Marine Leclerc[1], Nathalie Droin[5], Vincent de Montpréville[1,6], Olaf Mercier[6], Pierre Validire[7], Jean-Yves Scoazec[5], Christophe Massard[8], Salem Chouaib[1], David Planchard[2], Julien Adam[1#], Benjamin Besse[2#] and Fathia Mami-Chouaib[1,9§]

[1] INSERM UMR 1186, Integrative Tumor Immunology and Immunotherapy, Gustave Roussy, Fac. de Médecine - Univ. Paris-Sud, Université Paris-Saclay, 94805, Villejuif, France

[2] Department of Cancer Medicine, Gustave Roussy, Institut d'Oncologie thoracique, Gustave Roussy, Université Paris-Saclay, 94805 Villejuif, France

[3] Gastrointestinal and Medical Oncology Department, Hôpital Européen Georges Pompidou, Paris, France

[4] INSERM Unit U981, Department of Experimental Pathology, Gustave Roussy, Université Paris-Sud, Université Paris-Saclay, 94805, Villejuif, France

[5] Department of Biology and Medical Pathology, Gustave Roussy, 94805, Villejuif, France

[6] Hôpital Marie-Lannelongue, Service d'Anatomie pathologique, 92350, Le-Plessis-Robinson, France

[7] Institut Mutualiste Montsouris, Service d'Anatomie pathologique, 75014, Paris, France

[8] Drug Development Department, Gustave Roussy, Université Paris-Saclay, 94805, Villejuif, France

[9] Lead contact

[&] Current address, Laboratory of Translational Genomics and Targeted Therapeutics in Solid Tumors, August Pi i Sunyer Biomedical Research Institute (IDIBAPS), Barcelona, Spain; Medical Oncology Department, Hospital Clínic, Barcelona, Spain

*, # Contributed equally to this work

[§] **Corresponding author**: Fathia Mami-Chouaib, INSERM UMR 1186, Gustave Roussy. 39, rue Camille Desmoulins, F-94805 Villejuif, France. Phone: +33 1 42 11 49 65, Fax: +33 1 42 11 52 88, e-mail: fathia.mami-chouaib@gustaveroussy.fr

Running title: Role of CD8 T_{RM} in NSCLC response to anti-PD-1

Keywords: CD8 T_{RM} cells, CTL, Tc17, lung cancer, anti-PD-1 immunotherapy

Abbreviations: CTL: cytotoxic T lymphocytes; ICB: immune checkpoint blockade; ICAM-1: intercellular adhesion molecule-1; LFA-1: lymphocyte function-associated antigen-1; mAb: monoclonal antibodies; NSCLC: non-small-cell lung carcinoma; ORR: objective response rate; iPFS: immunotherapy progression-free survival; PD-1: programmed cell death-1; pSTAT3: phosphorylated-STAT3; TCR: T-cell receptor; T_{Eff}: effector T cells; TIL: tumor-infiltrating lymphocyte; T_{RM}: resident memory T cells.

Abstract

Accumulation of $CD103^+CD8^+$ resident memory T (T_{RM}) cells in human lung tumors has been associated with a favorable prognosis. However, the contribution of T_{RM} to anti-tumor immunity and to the response to immune checkpoint blockade has not been clearly established. Using quantitative multiplex immunofluorescence on cohorts of non-small-cell lung cancer patients treated with anti-PD-(L)1, we show that an increased density of $CD103^+CD8^+$ lymphocytes in immunotherapy-naïve tumors is associated with greatly improved outcome. The density of $CD103^+CD8^+$ cells increases during immunotherapy in most responder, but not in non-responder, patients. $CD103^+CD8^+$ cells co-express CD49a and CD69 and display a molecular profile characterized by expression of PD-1 and CD39. $CD103^+CD8^+$ tumor T_{RM}, but not $CD103^-CD8^+$ tumor-infiltrating counterparts, express Aiolos, phosphorylated-STAT-3 and IL-17, demonstrate enhanced proliferation and cytotoxicity toward autologous cancer cells and frequently display oligoclonal expansion of TCRβ clonotypes. These results explain why $CD103^+CD8^+$ T_{RM} are associated with better outcome in anti-PD-(L)1-treated patients.

Introduction

Effective cancer immunotherapy requires generation of persistent tumor-reactive cytotoxic T lymphocytes (CTL) that continuously eliminate primary malignant cells and micro-metastases. Immune checkpoint blockade (ICB), in particular via anti-programmed cell death-1 (PD-1) and anti-PD-L1 neutralizing monoclonal antibodies (mAb), has led to improved outcome in non-small-cell lung cancer (NSCLC) patients by blocking the interaction of PD-1 inhibitory receptor on tumor-specific T cells with its ligand PD-L1 on target cells, thereby reactivating their anti-tumor effector functions. ICB, as a single immunotherapy agent, has demonstrated responses in up to 20% of patients with advanced NSCLC that failed platinum-based chemotherapy. In this context, clinical benefits of anti-PD-(L)1 therapy required that tumors be infiltrated by $CD8^+$ T lymphocytes expressing high levels of PD-1 and mediating tumor-mutation-derived neoantigen-specific responses[1,2]. However, little is known of the nature of these $CD8^+$ T lymphocytes, whether they belong to the memory pool of T cells, and whether they patrol through blood or are confined to tumor tissues where they are permanently retained. Recently, a lineage of $CD8^+$ memory T cells, called resident memory T (T_{RM}) cells, was localized in several human solid tumors, including NSCLC, and was associated with a favorable prognosis[3-8].

T_{RM} cells were initially identified in infectious diseases, where they were located at sites of pathogen entry so as to trigger optimized protection against viral re-infections[9]. They are distinct from central memory T (T_{CM}) and effector memory T (T_{EM}) cells due to their non-recirculating behavior and restricted localization in non-lymphoid peripheral tissues. Indeed, this memory T-cell subset lacks molecules such as S1pr1, Klf2, CCR7 and CD62L, enabling egress from tissue and migration to lymph nodes, and has a unique surface phenotype characterized by expression of the CD69 activation marker, and CD103 (α_E(CD103)β_7) and CD49a (α_1(CD49a)β_1) integrins,

which likely participate in their residency feature by binding to E-cadherin and type IV collagen on epithelial and endothelial cells, respectively[10,11]. T_{RM} cells also upregulate lymphocyte-function-associated antigen-1 (LFA-1 or α_L(CD11a)β_2) integrin, which sustains their residence in liver tissue by binding to intercellular adhesion molecule-1 (ICAM-1) on endothelial cells[12]. Formation and persistence of anti-viral T_{RM} are regulated by a specific repertoire of transcription factors, including Runx3, Blimp-1, Hobit (homolog of Blimp-1 in T cells) and Notch, and involve a specific set of cytokines, including TGF-β, IL-15, Type I IFN and IL-12[13-15]. T_{RM} have been shown to produce pro-inflammatory cytokines such as IFNγ and TNF and cytotoxic serine protease granzyme B, which participate in recruiting other immune cells at sites of infection and mediating cytotoxic function, respectively. With regard to cancer diseases, much less is known about the generation and maintenance of T_{RM} at the tumor site and their role in anti-tumor immune responses. Thus far, the phenotypic and functional features of human tumor T_{RM} and their contribution to T-cell immunity to cancer and responses to ICB are poorly understood. In this report, we show that human lung tumor $CD8^+$ T_{RM} cells are a homogenous $CD103^+CD49^+CD69^+$ population characterized by expression of T-bet, phosphorylated (p)STAT-3 and Aiolos transcription factors, and that a subset of them produces IFNγ and IL-17, specific to Tc17 cells. NSCLC $CD8^+$ T_{RM} also produce granzyme B, form stable conjugates with autologous tumor cells, and mediate specific cytotoxic activity toward the cognate target. This tumor T_{RM} subset, but not its $CD103^-CD8^+$ tumor-infiltrating counterpart, proliferate and clonally expand in some tumors, suggesting that it is enriched in tumor-specific $CD8^+$ T cells. Remarkably, an enhanced $CD103^+CD8^+$ subset within the tumor microenvironment (TME) is associated with better progression-free survival (PFS) of anti-PD-(L)1-treated NSCLC patients. This subset is increased upon anti-PD-1 administration in tumors from most responder patients, but not in tumors from non-responder patients, and represents the major $CD8^+$ tumor-infiltrating

lymphocytes (TIL) population in intraepithelial tumor regions. Thus, $CD103^{+}CD8^{+}$ T_{RM} cells could be considered potential biomarkers when selecting patients who might benefit from ICB.

Results

Accumulation of CD103$^+$CD8$^+$ cells in tumors is associated with better outcome in anti-PD-(L)1-treated NSCLC patients

To determine the contribution of T_{RM} cells to the response to ICB, we established a retrospective tumor cohort (discovery cohort) of 111 patients with advanced NSCLC treated with single-agent anti-PD-(L)1 mAb (Table S1). Tumor sections from FFPE samples were stained simultaneously with anti-CD8, anti-CD103 and anti-cytokeratin mAb, and the density and distribution of CD103$^+$CD8$^+$ TIL and CD103$^-$CD8$^+$ TIL in epithelial and stromal regions were assessed using InForm software (Figure 1A). Among the 111 analyzed tumor samples, conclusive staining for quantification of CD103$^+$CD8$^+$ TIL was obtained for 86 patients. Multiplex fluorescent immunohistochemistry (IHC) revealed that the density of the CD103$^+$CD8$^+$ TIL subset varied between tumors, ranging from 0 to 1,320 cells/mm^2, with a median of 103 cells/mm^2. Most CD103$^+$CD8$^+$ TIL were located within the stroma, with a median density of 153 cells/mm^2. In epithelial tumor regions, there were fewer lymphocytes than in the stroma (median density of 68 cells/mm^2); however, 76% of these CD8$^+$ TIL were CD103$^+$ (median density of 45 cells/mm^2), whereas only 48% in the stroma (Table S1). Increased intraepithelial lymphocyte infiltration was particularly observed in tumors with a high density of CD103$^+$CD8$^+$ cells in the stromal compartment (Figure S1A).

We then correlated survival of patients from date of first immunotherapy administration with the score of tumor infiltration by CD8$^+$ TIL. In this cohort, the objective response rate (ORR) was 20% (n=17/86), corresponding to responders. As expected, patients with strong CD8 cell (CD8^{high}) tumor infiltration had increased survival compared to patients with CD8^{low} tumors (HR=0.40, 95% confidence interval [CI], 0.20-0.77, p=0.006), and median immunotherapy

progression-free survival (iPFS) of 9.92 months (95% CI 2.73-not-reached) (Figure S1B and Table S2). The density of $CD8^+$ TIL was also higher in responder patients than in non-responders (Figure S1C). Remarkably, when patients were stratified by their tumor $CD103^+CD8^+$ cell infiltration, iPFS dramatically increased in the patient population harboring tumors strongly infiltrated by $CD103^+CD8^+$ cells ($CD103^+CD8^{+high}$), with median iPFS reaching 30 months (95% CI 2.73-not-reached) (Figure 1B and Table S2). The density of total $CD103^+CD8^+$ TIL also correlated with ORR (Figure 1C). In contrast, patients with tumors slightly infiltrated by $CD103^+CD8^+$ cells had only a 2.3-month (95% CI 1.68-5.03) median iPFS. Multivariate analyses showed that tumor infiltration by $CD103^+CD8^+$ cells was an independent factor in satisfactory prognosis, based on iPFS, with a HR of 0.39 (95% CI 0.18-0.85, p=0.01) (Table S3). Importantly, median iPFS in the $CD103^+CD8^{+high}$ population was 20 months longer than in the total $CD8^{+high}$ population (Table S2). As expected, PD-L1 expression by tumor cells correlates with a better PFS (Table S1). These results highlight the strong benefit of an enhanced $CD103^+CD8^+$ cell subset in tumors compared to the heterogeneous $CD8^+$ subset in the response to anti-PD-(L)1.

Correlation between intraepithelial $CD103^+CD8^+$ TIL, tumor E-cadherin and ICAM-1 expression and response to ICB

Next, we examined $CD8^+$ TIL in epithelial tumor regions where immune cells are in close contact with tumor cells. Patients with high intraepithelial $CD103^+CD8^+$ TIL responded more effectively to anti-PD-(L)1 than patients with low intraepithelial $CD103^+CD8^+$ infiltration (HR=0.52 95% CI 0.31-0.88, p=0.01) (Figure 1D). The density of intraepithelial $CD103^+CD8^+$ TIL also correlated with ORR (Figure 1E). Similar results were observed when analyzing total $CD8^+$ cell infiltrate in the epithelial compartment, predominantly composed of $CD103^+CD8^+$ TIL (Figures S1D and S1E). Correlation between an enhanced total (Figures S1F and S1G), but to a lesser extent

epithelial (Figures S1H and S1I), $CD103^+CD8^+$ subset with better PFS of anti-PD-(L)1-treated patients was confirmed in a second cohort (validation cohort) of 41 NSCLC including 10 (26%) responder patients (Table S4). In contrast, patients with increased intraepithelial $CD103^-CD8^+$ TIL did not respond efficiently to anti-PD-1, with a HR of 1.74 (95% CI 1.05-2.88, p=0.03), and no correlation was observed between density of intraepithelial $CD103^-CD8^+$ cells and ORR (Figures 1F and 1G). Since epithelial tumor region infiltration by either high numbers of $CD103^+CD8^+$ cells or low numbers of $CD103^-CD8^+$ cells was associated with better outcome, we stratified the cohort into three groups based on these two parameters. Using a CD103/CD8 score, we considered a group as satisfactory if both parameters were present ($CD103^+CD8^{+high}$ and $CD103^-CD8^{+low}$), intermediate if only one parameter was present ($CD103^+CD8^{+high}$ or $CD103^-CD8^{+low}$) and poor if neither was present ($CD103^+CD8^{+low}$ and $CD103^-CD8^{+high}$). Interestingly, the group with a satisfactory CD103/CD8 score had a median PFS of 26.2 months (95% 15.3-not-reached), versus 2.7 months (95% CI 1.7-7.3) for the group with an intermediate score and 1.38 month for the group with a poor score (95% CI 0.72-1.97) ($p<0.0001$) (Figure 1H and Table S2). In addition, anti-PD-1-long-responder patients (PFS > 6 months and overall survival (OS) > 12 months) displayed a higher frequency of $CD103^+$ cells among $CD8^+$ TIL than fast-progressor patients (defined by an "early death" occurring during the first 12 weeks after the beginning of ICB) (Figure 1I). A higher density of intraepithelial $CD103^+CD8^+$ TIL in anti-PD-1-long-responder patients than in fast-progressor patients was also obtained in the validation cohort (Figure S1J). More importantly, quantitative multiplex fluorescent IHC staining of tumors collected from 9 patients (5 from the validation cohort and 4 additional patients) before (2-to-25 weeks) and after anti-PD-1 administration, showed an increase in the density of epithelial $CD103^+CD8^+$ TIL in 4 out of 5 responder patients. In contrast, no expansion of this subset was observed in 4 out of 4 non-responder patients (Figure 1J and Table S5). An increase in total

$CD103^+CD8^+$ and total $CD8^+$ TIL was also observed in responder patients (Table S5). These results highlight the importance of an enhanced intratumoral $CD103^+CD8^+$ cells in response to anti-PD-(L)1 and support the conclusion of a role of this subset in patient outcome.

We then assessed expression of E-cadherin and ICAM-1, the respective ligands of CD103 and LFA-1 integrins, known to play a major role in strengthening the interaction between CTL and tumor cells following T-cell receptor (TCR) recognition of major histocompatibility complex (MHC)-class I-peptide complexes[16, 17]. Expression of E-cadherin on cancer cells from 105 evaluable tumor sections out of the 111 analyzed NSCLC was scored into four groups: scores 0 and 1 were considered low (12%, n=13/105) and scores 3 and 4 were high (88%, n=92/105) (Figure S2A and Table S6). Data analyses indicated that E-cadherin expression does not affect PFS, and no effect on the density of intraepithelial $CD103^+CD8^+$ TIL was observed (Figures S2B and S2C). Similarly, according to ICAM-1 expression on tumor cells from 101 evaluable tumor sections out of the 111 analyzed tumors, the population was classified into low and high groups (Figure S2D), with no impact observed on survival or infiltration by $CD103^+CD8^+$ cells in epithelial regions (Figures S2E and S2F). Nevertheless, for tumors combining an epithelial $CD103^+CD8^{+high}$ plus ICAM-1^{high} profile, median PFS increased up to 15.3 months (95% CI 9.63-not-reached) versus a median PFS of 3.8 months (95% CI 2.56-not-reached) observed for the epithelial $CD103^+CD8^{+high}$ plus ICAM-1^{low} profile (Figure S2G and Table S2). These results support the observation that CD103 promoted CD8 T-cell infiltration within epithelial tumor regions, and suggest that these $CD103^+CD8^+$ lymphocytes are tumor-reactive T_{RM} cells.

CD8$^+$ TIL from NSCLC are highly enriched in CD103$^+$CD49a$^+$CD69$^+$ T$_{RM}$

Experiments were next performed to delineate phenotypic and molecular features of CD103$^+$CD8$^+$ NSCLC TIL, and to determine whether they are a homogenous population or whether heterogeneity exists in expression of conventional T$_{RM}$ surface markers. With this aim, CD8$^+$ TIL from 39 freshly resected treatment-naïve early-stage NSCLC tumors were isolated and stained for CD3, CD8, CD103, CD49a and CD69, as well as the effector T-cell (T$_{Eff}$) surface marker KLRG1 (Figure S3A). Results indicated that the percentage of CD8$^+$ T cells displaying a CD103$^+$KLRG1$^-$ phenotype ranged from 18 to 81%, with a mean of 51%, while the percentage of CD8$^+$ T cells displaying a CD103$^-$KLRG1$^+$ T$_{Eff}$ phenotype ranged from 7 to 52%, with a mean percentage of 26% (Figure 2A). The mean percentages of CD103$^+$KLRG1$^+$ and CD103$^-$KLRG1$^-$ T-cell subpopulations were only around 10% and 12% of CD8$^+$ TIL, respectively. Notably, expression of CD103 inversely correlated with that of KLRG1 on CD8$^+$ TIL and appeared mutually exclusive (Figure 2B).

We then further characterized the CD103$^+$CD8$^+$ TIL subset by evaluating expression of CD69 and CD49a T$_{RM}$ markers. Results showed that over 90% of CD103$^+$CD8$^+$ T cells expressed CD69 and CD49a (Figure 2C, Figures S3A and S3B), and that expression of CD49a correlated with that of CD103 (Figure 2D). In addition, most CD103$^+$ TIL displayed a CCR7$^-$CD45RA$^-$ profile, characteristic of effector memory T (T$_{EM}$) cells (Figure S3C). In contrast, only 50% and 35% of KLRG1$^+$CD8$^+$ TIL expressed CD69 and CD49a, respectively (Figure 2C). This T-cell subset is more heterogeneous in CD45A expression and is mainly composed of CCR7$^-$CD45RA$^-$ T$_{EM}$ and CCR7$^-$CD45RA^{high} terminally differentiated (EMRA) T cells (Figure S3C). CD103$^+$CD49a$^+$CD69$^+$ CD8 T cells, hereafter called T$_{RM}$, are also present in adjacent healthy lung tissues, but at a lower frequency and lower expression level of CD69 than in autologous

tumor tissues (Figure 2E and 2F). In contrast, the KLRG1$^+$ CD8 T-cell subset, hereafter referred to as non-T_{RM}, is more abundant in healthy lung tissue than in the cognate tumor (Figure 2E). In addition, the number of T_{RM} cells per milligram of tissue is much higher in the tumor than in the cognate normal lung, with mean values of around 1,000 T_{RM}/mg of tumor versus 100 T_{RM}/mg of healthy lung (Figure 2G), with no correlation between the two tissue compartments within each patient samples (Table S7). These data support the conclusion that NSCLC are strongly infiltrated by a homogenous CD103$^+$CD49a$^+$CD69$^+$ CD8 T_{RM} subset, readily distinguishable from the KLRG1$^+$ CD8 T_{Eff} subset.

Molecular features of NSCLC CD8 T_{RM} cells

To determine the transcriptional profile of the tumor T_{RM} subset, we performed RNA-based next-generation sequencing (RNA-seq) of CD103$^+$CD8$^+$ and matched KLRG1$^+$CD8$^+$ T cells freshly isolated from TIL of 7 treatment-naïve early-stage NSCLC. Gene expression analyses performed with a p-value $\leq$0.05 revealed a large number of transcripts (n=2,958) differentially expressed in the two T-cell subsets, supporting the notion that they correspond to two divergent populations (Figure S3D). Among these transcripts, we identified a gene signature characteristic of antiviral T_{RM} and NSCLC T cells[5,13,18,19], including upregulation of *CXCR6* and *SIRPG* transcripts (Figure S3E, Table S8). A gene signature with upregulation of *GPR34*, *ITGAE* and *CXCR6* genes and downregulation of *SIPR5* and *SIPR1*, encoding sphingosine phosphate receptors, *KLF2*, encoding Krüppel-like transcription factor that regulates T-cell trafficking, and *SELL,* encoding L-selectin CD62L, important in lymphocyte homing to lymphoid organs, was identified in tumor T_{RM} (Figure S3F and Table S8). Downregulation of S1pr1 in tumor CD103$^+$CD8$^+$ T_{RM} was confirmed by multiparametric flow cytometry, with levels similar to those of healthy lung T_{RM} (Figure S3G). In addition, gene set enrichment analysis (GSEA) showed that several hallmark gene sets,

such as inflammation, cell cycle, TGF-β signaling pathways, mammalian target of rapamycin (mTOR) and hypoxia, were enriched in T_{RM} (Figures S4A and S4B, and Table S9).

Among T_{RM} signature genes, a panel of genes involved in T-cell exhaustion, including *CTLA-4*, *BTLA*, *HAVCR2, PDCD1, LAG3* and *TIGIT,* were more strongly expressed in $CD103^+$ than in $KLRG1^+$ TIL subsets (Figure 3A, Figure S4C and Table S8). Upregulation of *SPRY1* (Sprouty), *ENTPD1* (CD39), *LAYN* (Layilin) and *TOX* genes was also observed in T_{RM} (Figure S4C). Flow cytometry analyses confirmed enhanced expression of PD-1 on T_{RM} cells from tumors, but not on non-T_{RM} and T_{RM} from cognate healthy lung tissue (Figure 3B). Notably, ectonucleotidase CD39 was specifically expressed by T_{RM}, and its expression was associated with PD-1 (Figure 3C and Figure S4D). Moreover, t-SNE analysis highlighted strong correlation of expression of CD39 and PD-1 with the T_{RM} cluster, whereas the non-T_{RM} cluster showed a weak association with these markers (Figure 3D). Expression levels of CD103 on $CD8^+$ TIL correlated with CD39 and 4-1BB (CD137) levels, and $CD103^{high}$ T cells also displayed $CD39^{high}$ (Figure 3E) and $4\text{-}1BB^{high}$ (Figure 3F) expression profiles characteristics of antigen-experienced T lymphocytes[20,21]. As expected, T_{RM} cells from adjacent normal lung expressed only low levels of 4-1BB, excluding recent engagement of TCR with specific antigen (Figure 3F). These results support the hypothesis that NSCLC $CD103^+CD8^+$ TIL were enriched with tumor-reactive T cells harboring all features of activated T_{RM}.

Lung tumor T_{RM} express transcription factors involved in Th17 differentiation

To explore potential pathways involved in T_{RM} formation in tumors, we studied genes encoding transcription factors differentially expressed in $CD103^+CD8^+$ and $KLRG1^+CD8^+$ TIL. RNAseq analyses indicated that $CD103^+CD8^+$ T cells displayed a specific signature characterized by

upregulation of *ZEB1* encoding the zinc-finger E-box binding homeobox-1*, ZNF683* (zinc-finger 683) encoding the Blimp1 homologue Hobit, and *PRDM1* (BLIMP1), and downregulation of *EOMES, IKZF2* (*HELIOS*), and *TCF7* genes (Figures 4A and 4B, Figure S5A, Table S8). Remarkably, a set of genes encoding transcription factors involved in Th17 differentiation, such as *IKZF3* encoding the Ikaros transcription factor family member Aiolos, and *AHR* encoding an aryl hydrocarbon receptor, were more strongly expressed in T_{RM} than in non-T_{RM} (Figure 4B and Figure S5A). A panel of genes associated with the Aiolos pathway, including *SMARCA4*, *UBE2I* and *GRAP2,* were also upregulated in T_{RM} (Figure S5B).

Flow cytometry analyses showed that tumor T_{RM} cells expressed lower levels of Hobit protein than non-T_{RM}, but levels higher than in healthy lung T_{RM} (Figure 4C). Downregulation of the *TCF7* gene-encoding protein TCF-1 in tumor T_{RM} as compared to non-T_{RM} was confirmed at the protein level (Figure 4D). In contrast, T-bet and Aiolos transcription factors were more strongly expressed in tumor T_{RM} than in non-T_{RM}, at levels similar to or higher than in healthy lung T_{RM} (Figure 4E). Moreover, AhR protein and phosphorylated-STAT3 (pSTAT3), also known as master regulators of Th17 differentiation, were more strongly expressed in T_{RM} than in non-T_{RM}, and at levels similar to those of healthy lung T_{RM} (Figures 4F and 4G, Figure S5C). Notably, tumor T_{RM} displaying high levels of CD103 ($CD103^{high}$) expressed higher levels of pSTAT3 than T_{RM} with intermediate ($CD103^{Int}$) and low ($CD103^{low}$) CD103 expression (Figure 4G). In addition, tumor T_{RM} expressed similar levels of pSTAT3 and Aiolos than healthy donor Th17-positive control cells (Figures 4E and 4G). In contrast, AhR was more strongly expressed in Th17-positive controls than in tumor T_{RM} (Figure 4F). The transcription factor RORγt was equally expressed by T_{RM} and non-T_{RM}, and the chemokine receptor CCR6 was more strongly expressed in T_{RM} than in non-T_{RM} (Figure S5D and Table S8). These results demonstrate that,

together with T-bet, human lung tumor CD8$^+$ T_{RM} express Aiolos, AhR and pSTAT3, three master regulators of the Th17 pathway, and ultimately suggest that they are enriched with Tc17 lymphocytes.

Lung tumor CD8$^+$ T_{RM} cells contain Tc17 and tumor-reactive CTL

To gain further insight into the molecular characteristics of human lung tumor CD8$^+$ T_{RM}, we studied expression profiles of genes involved in T-cell activation. Results showed that T_{RM} displayed a signature of more activated lymphocytes than non-T_{RM} (Figure 5A). Notably, GSEA highlighted upregulation of several genes belonging to the Th17/Tc17 cell lineage in T_{RM} (Figure 5B, Table S8). Among these genes, *IL17A* and *IL17RA*, encoding IL-17 and the IL-17 receptor (IL-17R), were more strongly expressed in T_{RM} than in non-T_{RM} (Figure 5C and Table S8). Upregulation of *IL17A* transcript in some T_{RM}, but not in non-T_{RM}, was further confirmed by RT-qPCR using paired CD103$^+$CD8$^+$ and KLRG1$^+$CD8$^+$ T cells from six additional lung TIL (Figure S5E). Moreover, intracellular flow cytometry analysis of fresh TIL stimulated *ex-vivo* with PMA plus ionomycin showed production of IL-17 by T_{RM} and healthy donor Th17-positive control cells, but not by non-T_{RM} cells (Figure 5D). Remarkably, higher percentages of IL-17-producing cells were observed in CD103^{high} T_{RM} than CD103^{int} and CD103^{low} (Figure S5F), and expression of CD39 and 4-1BB was frequently higher in IL-17$^+$ than IL-17$^-$ T_{RM} (Figure S5G). ELISA also confirmed restricted secretion of IL-17 in supernatants from T_{RM}, but not from non-T_{RM} (Figure 5E). In contrast, both non-T_{RM} and T_{RM} from tumors were able to produce high levels of IFNγ and TNFα following *ex vivo* stimulation with PMA plus ionomycin (Figure 5F). Moreover, a subset of T_{RM} cells from lung tumors produced both IL-17 and IFNγ (Figure 5G). These IL-17-producing CD8$^+$ T cells were not TCRγδ lymphocytes, which often display a CD4$^-$CD8$^-$ profile

and represent around 3.6% of $CD3^+$ TIL, only 2.2% of them produced IL-17 (Figures S5H and S5I)

Flow cytometry analyses showed that tumor T_{RM} expressed higher levels of proliferation marker protein Ki67 compared to tumor non-T_{RM} and T_{RM} from adjacent healthy lung (Figure 6A). Intracellular immunofluorescence also revealed that tumor T_{RM} expressed higher levels of granzyme B than non-T_{RM} and healthy lung T_{RM}, supporting the hypothesis that they are tumor-reactive CTL (Figure 6B). Consistently, further functional studies by confocal microscopy showed that tumor T_{RM} formed more stable conjugates with autologous cancer cells than non-T_{RM}, as evaluated by tyrosine phosphorylation (pTyr) at the contact zone between T cells and target cells (Figure 6C). Moreover, tumor T_{RM} were able to kill autologous tumor cells much more efficiently than non-T_{RM} (Figure 6D). These results further support the conclusion that T_{RM} infiltrating NSCLC tumors are activated tumor-specific cytotoxic effectors.

Lung tumor $CD8^+$ T_{RM} express a more clonal TCR repertoire than non-T_{RM}

To assess clonality of NSCLC $CD8^+$ T_{RM}, we investigated the TCRβ repertoire of nine freshly sorted $CD103^+CD8^+$ TIL and autologous $KLRG1^+CD8^+$ TIL by deep TCR sequencing. Results indicated that tumor T_{RM} were more oligoclonal than paired non-T_{RM} (Figure 7A and Figure S6A). Indeed, the ten most frequent (Top 10) TCRβ clonotypes, defined by hypervariable complementarity-determining region 3 (CDR3) nucleotide sequences, accounted for over 60% of the T_{RM} population and less than 45% of the non-T_{RM} (Figure 7B). In contrast, only a marginal difference was observed between TCRβ repertoires of T_{RM} cells from NSCLC tumors and proximal healthy lung (Figure S6B). TCRVβ family distribution within each T-cell subset was variable across patients, but it was different between T_{RM} and non-T_{RM} from a given patient

(Figure 7C). However, T_{RM} and non-T_{RM} populations shared some clonotypes, the proportions of which varied from one patient to another and ranged from 4% to 28% (Figures S6C-E). Next, we questioned whether the restricted TCRβ repertoire observed in T_{RM} cells correlated with expression of PD-1, reported to identify the $CD8^+$ tumor-specific repertoire infiltrating human tumors[22]. Data revealed a correlation between productive frequency of the top 10 clonotypes and the percentage of PD-1^+ $CD103^+CD8^+$ TIL (Figure 7D), further supporting the conclusion that NSCLC $CD8^+$ T_{RM} are an oligoclonal subpopulation enriched with activated tumor-specific T cells that underwent antigen-driven expansion at the tumor site. They also explain how this tumor-resident CTL subset can locally participate in anti-tumor CD8 T-cell immunity and contribute to the response to anti-PD-1 therapy.

Discussion

In this report, we show that NSCLC tumors are strongly infiltrated by $CD8^+$ T_{RM} cells, most of which express a homogenous $CD103^+CD49a^+CD69^+$ phenotype. This T_{RM} subset was also found in adjacent healthy lung tissues, but at lower densities than in autologous tumor samples, with no correlation between the frequency of either, suggesting that they are two distinct T_{RM} subsets. Tumor $CD103^+CD8^+$ TIL displayed transcriptomic and phenotypic signatures characteristic of T_{RM}, including downregulation of: 1) Klf2, that regulates genes involved in T-cell trafficking, such as *SELL*, *CCR7* and *S1PR1*[23]; 2) S1pr1, that mediates egress of T cells from lymphoid organs[24]; and 3) CD62L and CCR7, key regulators of T-cell migration to lymphoid organs, and upregulation of: (a) CD103, that favors T-cell recruitment and retention in epithelial tumor islets through binding to its ligand, epithelial cell marker E-cadherin[25]; (b) CD49a, responsible for retaining CD8 T_{RM} in peripheral tissues via attachment to the extracellular matrix[11]; and (c) CD69 C-type lectin that modulates T_{RM} cell capacity to exit non-lymphoid tissues through interaction and degradation of S1pr1[26]. NSCLC $CD8^+$ T_{RM} also overexpress several T-cell inhibitory receptors and exhaustion surface markers, with co-expression of PD-1 and CD39, supporting the conclusion that they are enriched in activated tumor antigen-reactive T cells. In this regard, it has been demonstrated that PD-1 accurately identifies the repertoire of clonally expanded tumor-specific $CD8^+$ T cells[22]. Expression of CD39, together with CD103, has been reported to identify truly tumor-reactive CD8 T cells in human solid tumors[20] and to distinguish tumor antigen-specific $CD8^+$ T cells from viral antigen-specific bystander T cells present in the TME[27]. The *TOX* gene, recently identified in tumor-reactive murine T cells and in human $PD1^{hi}CD39^{hi}$ TIL[28], was also upregulated in human NSCLC T_{RM}, further indicating that they are enriched in tumor-specific T cells. NSCLC T_{RM} also frequently expressed 4-1BB (CD137) costimulatory receptor characteristics of antigen-experienced TIL[21]. These molecular features

likely cooperate in retaining $CD8^+$ T_{RM} in tumor tissues to detect and mount robust local immune responses to transformed cells.

T-bet, together with Eomes T-box transcription factors, were demonstrated to control development and survival of skin and lung $CD103^+$ T_{RM} by controlling TGF-β and IL-15 expression[29]. However, while extinguishing Eomes is necessary for $CD103^+CD8^+$ T_{RM} cell formation, residual T-bet expression is required for IL-15-mediated $CD103^+CD8^+$ T_{RM} survival. Consistently, we show that lung tumor $CD103^+CD8^+$ T_{RM} express T-bet at levels similar to healthy lung $CD103^+CD8^+$ T_{RM}, but they only weakly express Eomes. *ZEB1* was strongly expressed in human NSCLC $CD103^+CD8^+$ T_{RM}, and this expression is likely induced by TGF-β at the tumor site. In this regard, Zeb1 has emerged as a critical transcription factor for memory T-cell survival and function[30]. At least a subset of NSCLC $CD8^+$ T_{RM} cells displays a transcription factor profile characteristic of Th17/Tc17 lymphocytes, with expression of Aiolos, pSTAT3 and AhR. Upregulation of Aiolos by STAT3 and AhR was reported to promote Th17 differentiation by silencing IL-2 expression[31]. In contrast, *TCF7*/TCF-1 was less abundant in NSCLC T_{RM} than in non-T_{RM}. Downregulation of *TCF7*/TCF-1 in $CD103^+CD8^+$ TIL is consistent with previous single-cell analyses of T_{RM} from breast cancer and NSCLC[7,8]. Exhausted $PD1^+CD8^+$ TIL from human melanoma are also *TCF7*^{neg} and enriched with CD39- and CD103-expressing cells[20,32]. Notably, activation of TCR leads to downregulation of TCF-1 in human $CD8^+$ T cells[33], suggesting recent TCR engagement of TCF-1^{low} NSCLC T_{RM}. These TCF-$1^{low/neg}$ $CD8^+$ cells, as opposed to bystander TCF-1^+ TIL, are tumor-reactive CTL[8,20,32,34], highlighting their antitumor potential and suggesting that TCF-1-expressing (stem-like or memory-precursor-like) cells are not the only source of T-cell expansion following ICB[35-40], and that TCF-1^{low} (T_{RM}) cells are also reactivated to participate to response to anti-PD-1.

TCF7 emerges as a central transcription factor in $CD8^+$ T_{RM} differentiation in IL-17-producing lymphocytes, as its downregulation results in enhanced Tc17-cell development[41]. Consistently, our functional experiments showed that a small subset of NSCLC $CD8^+$ T_{RM} cells produces IL-17 after PMA/ionomycin stimulation at frequency similar to heathy donor Th17/Tc17-polarized T cells. Human $CD8^+CD49a^-$ T_{RM} cells were also found to produce IL-17 in skin epithelia and psoriasis lesions, promoting local inflammation[42]. Differentiation of a subpopulation of $CD8^+$ T_{RM} cells into the Tc17 lineage is likely associated with secretion of IL-6 and TGF-β by lung tumor cells themselves, and inhibition of IFNγ, conditions known to promote formation of murine $CD4^+$ Th17 lineage[43]. Murine Tc17/IFNγ $CD8^+$ T cells mediate improved anti-tumor immunity associated with enhanced survival[44]. A small subset of NSCLC $CD103^+CD8^+$ T_{RM} also produces IL-17 and IFNγ, displays increased proliferative potential and mediates cytotoxic function toward autologous cancer cells correlated with production of granzyme B and formation of stable conjugates with the cognate target.

The notion that CD103 is a marker of antigen-specific T cells is supported by studies of antiviral and anti-tumor CTL responses, demonstrating that the integrin is induced on $CD8^+$ T cells specific to influenza virus in the lung[45], EBV in the tonsil[46], cancer testis antigen NY-ESO-1 in ovarian cancer[47] and the α-actinin 4 (actn-4) neoepitope in NSCLC[48]. Tumor antigen specificity of $CD103^+CD8^+$ T_{RM} cells was further emphasized by TCRseq analyses revealing expansion of particular TCR clonotypes in $CD103^+CD8^+$ TIL, but to a lesser extent in $KLRG1^+CD8^+$ TIL. TCR clonality in tumor $CD8^+$ T_{RM} correlated with high PD-1 expression, which reflects their strong activation state and suggests high TCR avidity for the tumor antigen, resulting in antigen-driving T-cell proliferation. Remarkably, $CD103^+CD8^+$ T_{RM} cells were shown to expand during

anti-PD-1 immunotherapy of melanoma[49] and lung carcinoma patients[8]. Here we provide evidence that a high density of $CD103^+CD8^+$ T_{RM} cells in tumors was associated with greatly improved PFS in NSCLC patients treated with anti-PD-(L)1 as single agent. We also provide evidence that the density of $CD103^+CD8^+$ TIL was increased in tumors after anti-PD-1 treatment, suggesting that PD-1 blockade reactivates this tumor-specific T_{RM} subset, which proliferates and exerts cytotoxic activity so as to participate to anti-tumor immunity and response to ICB. The reason for intertumor T_{RM} density variation is not understood, but it may reflect interpatient variations in the number of antigen-specific T-cell precursors, the tumor mutational burden or the amount of active TGF-β required for CD103 expression in TCR-engaged T lymphocytes[16,48,50]. With regard to epithelial tumor regions, enhanced infiltration by $CD103^+CD8^+$ T_{RM} did not correlate with E-cadherin expression levels by cancer cells. Consistent results were obtained in ovarian cancer[3], but not in bladder cancer where intratumoral infiltration of $CD103^+$ TIL was associated with expression of E-cadherin on tumor cells[51]. Although enhanced expression of ICAM-1 on cancer cells was not associated with increased density of $CD103^+CD8^+$ TIL in epithelial tumor islets, the combination with high T_{RM} infiltration improved patient PFS. This might be associated with strong adhesion between tumor cells and specific T_{RM} provided by the ICAM-1-LFA-1 interaction, and required for effective target cell lysis by activated CTL[17,52]. In contrast, infiltration of epithelial tumor regions by $CD103^-CD8^+$ TIL did not result in improved survival of anti-PD-1-treated patients. This is surprising, since previous studies reported that $CD8^+$ T-cell infiltration is associated with better clinical outcome and response to ICB[1]. Although the status of $CD8^+$ TIL for CD103 expression was not investigated, these T cells likely expressed the integrin, since CD103 is required for their recruitment and functionality within epithelial tumor regions[53].

Overall, our study demonstrates a major role for $CD103^+CD8^+$ T_{RM} cells in anti-tumor immunity and the response to anti-PD-1 in lung cancer. It also delineates CD103 as a biomarker able to accurately identify the repertoire of clonally expanded tumor-reactive $CD8^+$ T cells, that are activated, proliferate, a subset of which can produce IL-17 and IFNγ, and effectively kill autologous malignant cells. Thus, investigating $CD103^+CD8^+$ T_{RM} in cancer patients not only contributes to our understanding of the local anti-tumor CTL response, but also provides insight into the role of this T-cell population in response to ICB. Improved responses to anti-PD-1 in patients with high densities of tumor $CD103^+CD8^+$ T_{RM} cells, even after having undergone resection of their tumor, may be associated with a pool of cancer-specific $CD8^+$ T cells present in bone marrow, as described in infectious diseases[54]. This non-circulating memory $CD8^+$ T-cell subset develops in response to a wide variety of antigens, including tumor antigens, and expands upon antigen re-challenge. Thus, $CD103^+CD8^+$ T_{RM} appear to be crucial components in immune protection against cancer and in the response of NSCLC to ICB, opening up new avenues in cancer immunotherapy.

Limitations of Study

The total $CD8^{+high}$ population in the stroma was as correlative as the $CD103^+CD8^{+high}$ population (both with 30.62 months PFS) most likely due to the frequent expression of CD103 on $CD8^+$ TIL even in the stroma. The study lacks functional features on IL-17-producing T_{RM} cells. Isolation from the same tumor of IL-17-positive and IL-17-negative $CD8^+CD103^+$ TIL and sufficient number of autologous tumors cells will help to further characterize this small T_{RM}-cell subset. Single-cell RNAseq of the tumor T_{RM} population might help defining molecular features of Tc17 cells. TCRγδ lymphocytes may contribute to IL-17 production in the TME even though their total number is very weak.

Acknowledgments

This work was supported by grants from the "Institut National du Cancer" (INCa; PLBIO016-080 grant number 10557); the "Association pour la Recherche sur le Cancer" (ARC; grant numbers: PJA20161204720, SIGN'IT20181007792 and PJA 20181208049), "Ligue contre le Cancer" (Comité des Yvelines, grant number 9FI12414QLCZ and Comité du Val de Marne, 2019) and Bristol-Myers Squibb (BMS, France; grant number CA209-942). S Corgnac was supported by a grant from the "Groupement des Entreprises françaises dans la Lutte contre le Cancer" (GEFLUC; Grant number 2016-R16180LL) and Cancéropôle Ile de France, and was a recipient of a fellowship from FRM (Fondation Recherche Medicale), Gustave Roussy (SIRIC-SOCRATE) and INCa (PLBIO016-080 grant number 10557). IM was a recipient of a fellowship from the Ligue National contre le Cancer. ML was a recipient of a MENRT fellowship from the French Ministry of Research, a fellowship from the Ligue contre le Cancer and Gustave Roussy (SIRIC-SOCRATE), and a "Taxe d'apprentissage" TA-2016 from École des Sciences du Cancer de Gustave Roussy/Université Paris-Sud. We thank Georges Bismuth from Cochin Hospital and Eric Tartour from Hôpital Européen Georges Pompidou for critically reading this manuscript. We also thank Yann Lecluse and Philippe Rameau from the cytometry facility (Plateforme d'Imagerie-Cytométrie), Virginie Marty from the platform of histocytopathology (Centre de Ressources biologiques, CRB), and Yahia Adnani and Guillaume Meurice from the platform of Bioinformatics (INSERM US23, CNRS UMS3655) of Gustave Roussy for their help with flow cytometry, lung tumor specimens and RNA sequence analyses, respectively. We are grateful to José-Carlos Benitez-Montanez, Jihène Lahmar-Bach-Hamba, Jordi Remon-Masip, Maud Ngocamus and Claudio Nicotra from the Department of Cancer Medicine of Gustave Roussy for their help in establishing patient tumor cohorts. We also thank Vassili Soumelis from Institut Curie, for his help with RNA extraction protocol and Caroline Communaux from the CRB of

Marie Lannelongue Hospital for her help with fresh human NSCLC tumors. Graphical abstract has been created with BioRender.

Author Contributions

Conception and design: S.C and F.MC Development of methodology: S.C, I.M, N.D, J.A. and F.M.C Acquisition of data (providing animals, acquiring and managing patients, providing facilities, etc.): S.C., I.M., L.M., E.A., H.H., T.D., M.L., E.V., J.K., L.G., N.S., P.V., V.M., O.M., JY.S., C.M., S.C., D.P., J.A., B.B. and F.MC. Analysis and interpretation of data (e.g., statistical analysis, biostatistics, computational analysis): S.C., E.A., L.M., J.A., B.B. and F.MC. Writing, reviewing and/or revision of the manuscript: S.C and F.MC. Administrative, technical and material support (i.e. reporting and organizing data, constructing databases): S.C., I.M., L.M., E.A., P.V., V.M., O.M., JY.S., C.M., B.B. and F.MC. Study supervision: F.M.C

Declaration of Interests

Benjamin Besse's sponsored research at Gustave Roussy Cancer Center: Abbvie, Amgen, AstraZeneca, BeiGene, Blueprint Medicines, BMS, Boehringer Ingelheim, Celgene, Cristal Therapeutics, Daiichi-Sankyo, Eli Lilly, GSK, Ignyta, IPSEN, Inivata, Janssen, Merck KGaA, MSD, Nektar, Onxeo, OSE immunotherapeutics, Pfizer, Pharma Mar, Roche-Genentech, Sanofi, Servier, Spectrum Pharmaceuticals, Takeda, Tiziana Pharma, Tolero Pharmaceuticals.

All the other authors have no conflict of interest.

Figure legends

Figure 1. Increased $CD103^+CD8^+$ TIL are associated with improved outcome of anti-PD-1-treated NSCLC. (**A**) Fluorescent IHC image of CD8, CD103, cytokeratin and dapi staining in lung tumor section (up). Digital mark-up image shows epithelial and stromal zones of the tumor section defined by cytokeratin staining (middle). Digital mark-up image shows $CD103^+CD8^+$ (yellow), $CD103^-CD8^+$ (green), $CD103^+CD8^-$ (red) and $cytokeratin^+$ (pink) cells in lung tumors (down). Scale bar, 2 cm. (**B**) Kaplan-Meier curve shows iPFS of anti-PD-1-treated patients with tumors harboring high (>252/mm^2) (n=19) or low (<252/mm^2) (n=65) densities of $CD103^+CD8^+$ cells (n=84). (**C**) Density of total $CD103^+CD8^+$ cells in tumors depending on iORR of non-responders (NR) (n=65) and responders (R) (n=17) patients to PD-1 blockade. (**D**) Kaplan-Meier curve shows iPFS of anti-PD-1-treated patients with tumor epithelial regions harboring a high (> 48/mm^2) (n=40) or low (< 48/mm^2) (n=44) density of $CD103^+CD8^+$ cells (n=84). (**E**) Density of $CD103^+CD8^+$ cells in epithelial tumor regions depending on iORR of NR (n=65) and R (n=17) patients to anti-PD-1. (**F**) Kaplan-Meier curve shows iPFS of PD-1 blockade-treated patients with epithelial regions of tumors harboring a high (>17/mm^2) (n=43) or low (<17/mm^2) (n=41) density of $CD103^-CD8^+$ cells. (**G**) Density of $CD103^-CD8^+$ cells in epithelial tumor regions depending on iORR of NR (n=65) and R patients (n=17) to PD-1 blockade. (**H**) Kaplan-Meier curve shows iPFS of anti-PD-1-treated patients with tumors harboring a satisfactory ($CD103^+CD8^{+high}$/$CD103^-CD8^{+low}$, red, n=12), intermediate ($CD103^+CD8^{+high}$ or $CD103^-CD8^{+low}$, blue, n=57) or poor ($CD103^+CD8^{+low}$/$CD103^-CD8^{+high}$, black, n=15) CD103/CD8 score. (**I**) Percentages of $CD103^+$ cells among $CD8^+$ TIL in epithelial tumor areas of anti-PD-1-treated patients undergoing a long-response (PFS > 6 months and OS > 12 months; n=13) or a fast-progression (OS< 12 weeks; n=17). ** $p<0.01$. (**J**) Fluorescent IHC images show $CD103^+CD8^+$ (orange), $CD103^-CD8^+$ (green), $cytokeratin^+$ (pink) and $Dapi^+$ (blue) cells in tumors from responder and non-responder

patients before and after administration of anti-PD-1. Scale bar 1 cm. Right**,** density of $CD103^+CD8^+$ cells in epithelial tumor regions of tumors before and after administration of anti-PD-(L)1 in responder (n=5) or non-responder (n=4) patients. p-value was determined by log-rank test (**B, D, F** and **H**), Chi2 test (**C, E** and **G**) or unpaired t-test (**I**). See also Figures S1, S2 and Tables S1-6

Figure 2. Expression of CD103, CD49a and CD69 on CD8 T cells infiltrating treatment-naïve NSCLC and healthy lung tissues. (**A)** Freshly resected NSCLC tumors were dissociated, and the $CD8^+$ T-cell subset was analyzed for CD103 and KLRG1 expression. Representative dot plots from four different TIL samples are included (bi-exponential scale). Right, percentages of $CD103^+KLRG1^-$, $CD103^-KLRG1^+$, $CD103^+KLRG1^+$ and $CD103^-KLRG1^-$ TIL subsets among $CD3^+CD8^+$ cells (n=39). (**B)** Inverse correlation between percentage of $CD103^+$ and $KLRG1^+$ cells among $CD8^+$ TIL (n=40). The r value indicates Pearson correlation coefficient.
(**C**) Expression of CD69 and CD49a on $CD103^+$ and $KLRG1^+$ $CD8^+$ TIL. Representative dot plot from one TIL sample is shown. Right, percentages of $CD69^+$ and $CD49a^+$ cells among $CD103^+$ and $KLRG1^+$ CD8 TIL are presented (n=17 and n=16, respectively). (**D)** Correlation between percentage of $CD103^+$ and $CD49a^+$ cells among $CD8^+$ TIL (n=27). (**E)** Percentages of $KLRG1^+$ (n=16) and $CD103^+CD49^+$ cells (n=19) among $CD8^+$ T cells infiltrating tumors or autologous healthy lung tissues. (**F)** Percentages of $CD69^+$ cells among $CD103^+CD49a^+$ CD8 T cells from tumor or healthy lung tissues (n=19). **(G)** Total numbers of $CD103^+CD69^+CD49a^+$ CD8 (T_{RM}) cells per milligram (mg) of tumor tissues and paired normal lung (n=18). Each symbol represents individual TIL or lung sample; horizontal lines correspond to mean ± standard error of the mean (SEM). ** P<0.01, *** P<0.001 (paired t-test). See also Figure S3 and Table S7

Figure 3. Expression of T-cell exhaustion transcripts and proteins in T_{RM} cells from NSCLC tumors. (**A**) Heat map of transcripts involved in T-cell exhaustion differentially expressed in $CD103^+$ and $KLRG1^+$ $CD8^+$ TIL (n=7). Different expression patterns correspond to different isoforms of the same gene. (**B**) Expression of PD-1 on $CD103^+$ and $KLRG1^+$ $CD8^+$ TIL. Dot plots of one representative patient. Right, percentages of $PD\text{-}1^+$ cells among T_{RM} and non-T_{RM} (n=21) and paired T_{RM} from healthy lung (n=13). (**C**) Percentages of $CD39^+$ cells in paired T_{RM} and non-T_{RM} from NSCLC (n=13). (**D**) t-SNE map of $CD103^+CD49a^+$ (blue) and $KLRG1^+$ (pink) cells among $CD8^+$ TIL. Right, t-SNE analysis of CD39 and PD-1 expression on $CD103^+CD49a^+$ (T_{RM}) and $KLRG1^+$ (non-T_{RM}). Data are from two representative TIL samples (patients 3 and 4). (**E**) Dot plots of CD39 expression on $CD103^+CD8^+$ T_{RM}, displaying high ($CD103^{high}$), intermediate ($CD103^{int}$) and low ($CD103^{low}$) CD103 phenotype, and $CD103^-CD8^+$ TIL from one representative tumor. Right, percentages of $CD39^+$ cells among T_{RM} expressing high, int and low levels of CD103, and $CD103^-CD8^+$ TIL (n=16). (**F**) Dot plot of 4-1BB expression on $CD103^+CD8^+$ TIL from one representative tumor. Right, percentages of $4\text{-}1BB^+$ cells among T_{RM} displaying high, int and low CD103 profiles. $CD103^-CD8^+$ TIL (n=7) and $CD103^+CD8^+$ T_{RM} from autologous normal lungs (n=4) are included. CD103 intensity is shown by a gradient color code. Symbols represent individual TIL or lung samples; horizontal lines correspond to mean ± SEM. * $P<0.05$ ** $P<0.01$, *** $P<0.001$ (paired t-test or ANOVA with Bonferroni post-hoc test); ns, not significant. See also Figures S3, S4 and Table S8

Figure 4. Transcription factor profiles of T_{RM} and non-T_{RM} from NSCLC. (**A**) Heat map of transcripts encoding transcription factors differentially expressed in $CD103^+$ and $KLRG1^+$ $CD8^+$ TIL (n=7) (p-value<0.05). (**B**) Expression of *ZEB1*, *ZNF683* (HOBIT), *PRDM1* (BLIMP1), *IKZF3* (AIOLOS), *EOMES* and *AHR* genes in T_{RM} and non-T_{RM} from NSCLC (n=7). Values are

TPM. (**C**) Percentages of Hobit$^+$ cells among T_{RM} and non-T_{RM} from NSCLC (n=21) and among healthy lung T_{RM} (n=15). Right, expression of Hobit (gMFI) in T_{RM} and non-T_{RM} from NSCLC (n=21) and in healthy lung T_{RM} (n=15). (**D**) Expression of TCF-1 (gMFI) in tumor T_{RM} and non-T_{RM} (n=7). (**E**) Percentages of T-bet$^+$ cells among tumor T_{RM} and non-T_{RM} (n=21) and among healthy lung T_{RM} (n=11). Right, expression of Aiolos (gMFI) among tumor T_{RM} and non-T_{RM} and paired healthy lung T_{RM} (n=13). Heathy donor Th17 control cells are included (n=2). (**F**) Expression of AhR (gMFI) in tumor T_{RM} and non-T_{RM} (n=10), and in Th17-positive control cells (n=2). (**G**) Expression of pSTAT3 (gMFI) in tumor T_{RM} and non-T_{RM} (n=10), and in Th17-positive controls (n=2). Right, expression of pSTAT3 (gMFI) in tumor T_{RM} cells displaying CD103^{high} (High), CD103^{int} (Int) and CD103^{low} (Low) phenotype, and in CD103$^-$CD8$^+$ TIL (Neg) (n=10). Each symbol represents one individual donor; horizontal lines are mean ±SEM. * P<0.05 ** P<0.01, *** P<0.001 (paired t-test or ANOVA with Bonferroni post-hoc test). gMFI: geometric mean fluorescence intensity; ns: not significant. See also Figure S5 and Tables S8 and S9

Figure 5. A subset of tumor CD103$^+$ CD8$^+$ T_{RM} displays a Tc17-polarized pattern. (**A**) Heat map of activation gene signature differentially expressed in paired CD103$^+$ and KLRG1$^+$ CD8$^+$ TIL (n=7) (p-value < 0.05). (**B**) GSEA of gene set from Th17 signature in the transcriptome of CD103$^+$CD8$^+$ TIL relative to KLRG1$^+$CD8$^+$ TIL (n=7). Running enrichment score (RES) for the gene set as the analysis 'walks down' the ranked list of genes; the position of gene set members (black vertical lines) in the ranked list of genes and the value of ranking metric are shown.
(**C**) Expression of *IL17A* and *IL17RA* transcripts encoding IL-17 and IL17-R, respectively, in tumor T_{RM} and non-T_{RM} (n=7). TPM are shown. (**D**) Intracellular expression of IL-17 in CD8$^+$ TIL stimulated for 4 h with PMA plus ionomycin. One representative dot plot is shown. Right,

percentages of IL-17$^+$ cells among T_{RM} and non-T_{RM} from tumors (n=12). Healthy donor Th17 positive control cells are included (n=2). (**E)** Production of IL-17 measured by ELISA in supernatant of tumor T_{RM} and non-T_{RM} stimulated overnight with PMA plus ionomycin. Data are concentrations of IL-17 in pg/ml per 100,000 cells (n=5). (**F)** Intracellular expression of IFNγ and TNFα in CD8$^+$ TIL stimulated with PMA plus ionomycin. Dot plots from one representative patient are shown. Right, percentages of IFNγ$^+$ (n=13) and TNFα$^+$ (n=7) cells among T_{RM} and non-T_{RM} from tumors. (**G)** Intracellular co-expression of IL-17 and IFNγ in tumor T_{RM} stimulated with PMA plus ionomycin. Two representative patients are shown. Horizontal lines are mean ± SEM. * P<0.05; *** P<0.001 (paired t-test or ANOVA with Bonferroni post-hoc test). See also Figure S5 and Table S8.

Figure 6. T_{RM} are tumor-specific CD8$^+$ T cells. (**A**) Intracellular expression of Ki67 in T_{RM} and non-T_{RM} from NSCLC. Dot plot of one representative patient is shown. Right, percentages of Ki67$^+$ cells in paired T_{RM} and non-T_{RM} cells from tumors and paired T_{RM} from healthy lung (n=18). (**B)** Intracellular expression of granzyme B in tumor T_{RM} and non-T_{RM}. Dot plot of one representative patient is shown. Right, percentages of granzyme B$^+$ cells in T_{RM} and non-T_{RM} from tumors and paired T_{RM} from healthy lung (n=14). (**C**) Conjugates formed between freshly isolated CD8$^+$ tumor T_{RM} or non-T_{RM} and autologous tumor cells were analyzed by confocal microscopy for p-Tyr (green fluorescence) accumulation in the contact area. T cells were labeled with anti-CD8 mAb (red). Scale bars, 10 µm. Right, quantification of pTyr fluorescence intensity fold increase in CD8 T cells at contact zone with cognate target cells. Four representative patients are included. Each symbol represents an individual synapse from 15 to 37 analyzed conjugates. (**D**) Cytotoxic activity of freshly isolated tumor T_{RM} and non-T_{RM} toward autologous cancer cells

determined by a conventional 4 h chromium release assay at 20:1 E:T ratio. Data correspond to 4 independent experiments with 4 different tumor samples. Horizontal lines are mean ± SEM from triplicate. * $p<0.05$; *** $p<0.001$ (paired t-test or ANOVA with Bonferroni post-hoc test).

Figure 7. Tumor CD8$^+$ T_{RM} cells display an oligoclonal TCR repertoire. (**A**) Frequency of productive TCR sequences of the top ten clonotypes (grey) and all other clonotypes (white) in paired NSCLC T_{RM} and non-T_{RM} from each patient sample (P22 to P30). TCRβ CDR3 region in tumor T_{RM} and non-T_{RM} were analyzed by TCRseq (n=9). (**B**) Frequency of the top ten TCR sequences in tumor T_{RM} and non-T_{RM} from both TCRseq and RNAseq (n=14). (**C**) Pie charts illustrating distribution of TCRVβ families in T_{RM} and non-T_{RM} from tumors (n=9) and autologous T_{RM} from healthy lungs (n=4). (**D**) Correlation between productive frequency of the top ten TCR clonotypes and the percentage of PD-1$^+$ cells in tumor T_{RM} (n=11). Horizontal lines correspond to mean ± SEM. * $P<0.05$ paired t-test; ns, not significant. The r value indicates the Pearson correlation coefficient. See also Figure S6

STAR Methods

RESOURCE AVAILABILITY

Lead contact

Further information and requests for resources and reagents should be directly to and will be fulfilled by the Lead contact, Fathia Mami-Chouaib (fathia.mami-chouaib@gustaveroussy.fr)

Materials Availability

This study did not generate new unique reagents.

Data and Code Availability

The RNA sequencing dataset comparing the transcriptome of $CD8^+CD103^+$ cells with $CD8^+CD103^-$ cells, as shown in Figures 3, 4 and 5, Figures S3 and S4, Tables generated during this study are available at European Genome-phenome Archive (EGA) under (???? Ongoing submission) access number.

EXPERIMENTAL MODEL AND SUBJECT DETAILS

Patient cohort characteristics and tumor samples

We conducted a monocentric retrospective study of a discovery cohort of 111 and a validation cohort of 41 advanced NSCLC patients receiving treatment with PD-1/PD-L1 inhibitors in a variety of settings covering routine clinical care, expanded access, compassionate-use programs and clinical trials (nivolumab, pembrolizumab, atezolizumab or durvalumab) at Gustave Roussy between November 2012 and February 2020. Demographic, clinical, pathological and molecular data were also collected (Tables S1 and S4). Radiological assessments were performed every 8 weeks per RECIST v1.1 and per the investigator's discretion. Fast-progressors were defined as patients who died during the first 12 weeks since the start of immunotherapy. This study was approved by the Institutional Review Board of Gustave Roussy (Commission scientifique des

Essais thérapeutiques [CSET]) and informed consent was obtained. Freshly resected lung tumors and adjacent healthy lung tissue samples were obtained from the Institut mutualiste Montsouris and the Hôpital Marie-Lannelongue. For these resected tissues, the sex and the gender of the subjects are not known.

Healthy donor blood samples were collected from the French blood bank (Etablissement Français du Sang (EFS); agreement number N°12/EFS/079). The sex and the gender of the subjects are not known.

METHOD DETAILS

Immunohistochemical staining

IHC was performed on archived FFPE tumor tissues using Ventana Benchmark and Discovery automated platforms. Briefly, after deparaffinisation and epitope retrieval in CC1 buffer (pH=8, 36 min at 95°C), tissue sections were incubated with primary mAb for ICAM-1 (clone N1C2, GeneTex, 1:200 dilution) or E-cadherin (clone EP6, Bio SB, prediluted) for 1 h at room temperature. Amplification and detection steps used the ultraview kit with amplification, and 3,3'-diaminobenzidine was used as a chromogen. ICAM-1 staining was evaluated as H-score (0 to 300) based on the percentage of tumor cells stained at each intensity (scale from 0 to 3). Since the intensity of E-cadherin staining was homogenous within each individual tumor sample, we scored E-cadherin staining as the prominent intensity for each tumor on a semi-quantitative scale from 0 to 3.

Multiplexed fluorescent IHC for CD8 T_{RM} was performed by sequential staining of a single tissue section with anti-CD8 (clone SP16, Spring Bioscience, 1:200), anti-CD103 (clone EPR4166-2, Abcam, 1:200) and anti-cytokeratin (clones AE1/AE3, Agilent, 1:100). For each staining, the

HRP-conjugated amplification system was associated with a tyramide-coupled fluorophore: Opal 690, Opal 250 and Opal 570, respectively. Multispectral fluorescent images were captured using the Vectra 3 microscope (PerkinElmer) and regions of interest were selected. Image analysis using InForm software (PerkinElmer) included spectral unmixing, tissue segmentation (stromal versus epithelial areas) using a trainable classifier, nuclei detection based on dapi staining and cell segmentation followed by cell phenotyping for identification of cell populations defined by the combination of individual markers. The density (number of cells per square mm) of $CD8^+$, $CD103^+$ $CD8^+$ and $CD103^-CD8^+$ cells was determined for each tumor sample in the total tumor area, as well as in the stromal and intraepithelial compartments, based on tissue segmentation. Results from image analysis were validated for all cases.

Tumor cells and tissue-infiltrating lymphocytes isolation

Freshly resected lung tumors and adjacent healthy lung tissue samples were immediately cut into small fragments and digested for 40 min at 37°C using the tumor dissociation kit (Miltenyi Biotech). The dissociated samples were smashed on 100 µm cell strainers, washed, and red blood cell lysis was performed. CD8 T lymphocytes were positively selected using CD8 microbeads according to the manufacturer's instructions (Miltenyi Biotec). Recovered cells were either used for phenotypic analyses or further sorted by BD FACSAriaIII or BDFusion cell sorter (BD Biosciences) using anti-CD8-Pacific blue (RPA-T8, Biolegend), anti-CD103-FITC (Ber-ACT8, Biolegend) and anti-KLRG1-PE (clone 13F12F2, ebioscience) mAb. Dead cells were excluded using DAPI. $CD103^+CD8^+$ and $KLRG1^+CD8^+$ T-cell populations were isolated and then either stored at -80°C for further DNA or RNA isolation or cultured for 2-5 days in the presence of low doses of IL-2 (20 U/ml) for functional studies. Tumor cells were recovered from the negative

fraction of the CD8 T-cell isolation described above, and then purified using a human tumor cell isolation kit (Miltenyi Biotec).

RNA and TCR sequencing and analyses

Total RNA was extracted from each sorted $CD103^+CD8^+$ and $KLRG1^+CD8^+$ TIL population pair and autologous healthy lung $CD103^+CD8^+$ lymphocytes when available; 150,000 lymphocytes per sample were processed using a single cell RNA purification kit (Norgen) according to the manufacturer's instructions. RNA integrity (RNA Integrity Score ≥ 7.0) was checked on the Agilent 2100 Bioanalyzer and quantity was determined using Qubit (Invitrogen). The SureSelect Automated Strand-Specific RNA Library Preparation Kit was used according to the manufacturer's instructions with the Bravo Platform. Briefly, 50 ng of total RNA sample were used for poly-A mRNA selection using oligo(dT) beads and subjected to thermal mRNA fragmentation. The fragmented mRNA samples were subjected to cDNA synthesis and were further converted into double-stranded DNA using the reagents supplied in the kit, and the resulting dsDNA was used for library preparation. The final libraries were bar-coded, purified, pooled in equal concentrations and subjected to paired-end sequencing on a HiSeq-2000 sequencer (Illumina). Fast quality was assessed using FastQC (v 0.11.3) and did not require further trimming or adaptor removal. Counting of reads over the transcriptome was performed over Gencode (v 19, GRCh37.p13) with Salmon[55] (v 0.8.2), using non-oriented library, 100 bootstrap and sequence bias correction. All other parameters were left to default. The pseudo-mapping rates were between 79% and 88% of overall reads. Differential analysis was performed within the R (v 3.2.3) environment with sleuth[56] (v 0.28.1), wasabi (v 0.1) and in-house scripts. PCA highlights inter-individual variations that are far above any variation of interest, which was confirmed by a likelihood-test ratio and taken into account within the Wald test.

Primary functional analyses were performed using Ingenuity Pathway Analysis and GSEA was performed with clusterProfiler[57] (v 3.8.0). RNAseq are available at the European Molecular Biology Laboratory European Bioinformatics Institute database (https://www.ebi.ac.uk/arrayexpress). TCR repertoire analysis was performed with a MiXCR package[58] (v 2.1.10). KEGG pathway: http://www.genome.jp/kegg-bin/show_pathway?hsa04660.

For TCRseq, total DNA from $CD103^+CD8^+$ and $KLRG1^+CD8^+$ TIL subset pairs and autologous healthy lung $CD103^+CD8^+$ cells when available, sorted from nine NSCLC patient tissues, was purified using a QIAamp DNA micro kit (Qiagen). DNA was quantified with fluorescence-based measurement Qubit (Life Technologies). TCRβ-CDR3 sequencing was performed by ImmunoSEQ, Adaptive Biotechnologies (Seattle). Raw data of TCR reads and sequences were uploaded on the ImmunoSEQ Analyser Platform (Adaptive Biotechnologies).

For quantitative (q) RT-PCR, total RNA was extracted from sorted cell populations using the single cell RNA purification kit (Norgen Biotek). cDNA were synthesized using the Maxima first strand cDNA synthesis kit (Thermo-Fischer Scientific). qRT-PCR was performed on a step-one plus (Applied Biosystems) using Maxima SYBR Green Master Mix (ThermoFischer Scientific). Expression levels of transcripts were normalized to 18S housekeeping gene. PCR primers for human, *TCF7, IKZF3, AHR, RORC, IL17* and *18S* genes were designed by Sigma-Aldrich and used according to the manufacturer's recommendations (Table S10).

Flow cytometry and ELISA

Phenotypic analyses were performed by direct immunofluorescence with a panel of fluorochrome-conjugated antibodies. Anti-CD3-Alexa700 (UCHT1), anti-CD8-PacificBlue (RPA-T8), anti-CD69-APC-Cy7 (FN50), anti-granzyme-B-FITC (GB11), anti-TNFα-PE/Dazzle594 (Mab11), anti-Aiolos-Alexa488 (16D9C97), anti-Vα7.2-APC-Cy7 (3C10), anti-CD161-Alexa488 (HP-3G10), anti-TCF-1-PE (7F11A10), anti-4-1BB-PE-Dazzle594 (clone 4B4-1) and anti-TCRγδ-PerCPCy5.5 (B1) were supplied by BioLegend. Anti-CD103-BV711 (Ber-ACT8), anti-IFNγ-APC (B27) and anti-Hobit-Alexa647 (Sanquin-Hobit/1) was purchased from BD Biosciences, anti-KLRG1-PE (13F12F2), anti-CD49-PerCPefluor710 (TS2/7), anti-S1PR1-APC (SW4GYPP), anti-PD-1-PeCy7 (eBioJ105), anti-AHR-PerCPefluor710 (FF3399), anti-Ki67-PerCPefluor710 (20Raj1) were supplied by Thermo Fisher Scientific. Anti-CD45RA-APC, anti-pSTAT3pS727-APC, anti-CD39-APC, anti-IL17A-PeVio770 and anti-Tbet-APC (REA102) were purchased from Miltenyi. For intracellular expression of IFNγ, TNFα and IL-17A, cells were stimulated for 4 h with PMA (50 ng/ml) plus ionomycine (1 µg/ml) in the presence of BrefeldinA (1 µg/ml, ebioscience). Cells were fixed, permeabilized (FoxP3 buffers Kit, ebioscience) and then stained with fluorochrome-conjugated mAb. Dead cells were excluded using a LIVE/DEAD Fixable UV dead cell stain kit (Thermo Fisher Scientific). Stained cells were analyzed by flow cytometry using a BD FACS Fortessa flow cytometer (BD Biosciences). Data were processed using FlowJo V10 software (Tree Star Inc.).

For ELISA, sorted $CD8^+$ T lymphocytes were stimulated overnight with PMA plus ionomycine, and then supernatants were stored until IL-17 dosage (eBiosciences).

Th17-positive control cells were generated from healthy donor's $CD4^+$ peripheral blood lymphocytes (PBL) stimulated with anti-CD3 and anti-CD28 in the presence of TGF-β and IL-6.

Conjugate formation and cytotoxic experiments

Formation of stable conjugates between T cells and autologous tumor cells was analyzed by confocal microscopy. Effector and target cells were co-cultured for 30 min at 1:1 E:T ratio, and then plated on poly-(L-lysine)-coated coverslips (Sigma-Aldrich, Saint-Louis, MO). Cells were then fixed, permeabilized as described[16] and stained with mouse anti-phospho-tyrosine (PY20, BD Biosciences) and rabbit anti-CD8 (Thermo Fisher Scientific), followed by anti-mouse AlexaFluor-488 and anti-rabbit AlexaFluor-647 (Thermo Fisher Scientific). Coverslips were mounted and analyzed using a fluorescence microscope (Leica, HR Sp8) with x63 lenses, and polarization of phospho-Tyr to the immune synapse between T cells and target cells was calculated. Stable conjugates were defined by polarization of p-Tyr at the contact zone between effector cells and tumor cells. Cytotoxic activity was evaluated using the conventional 4 h ^{51}Cr-release assay as described[16].

QUANTIFICATION AND STATISTICAL ANALYSIS

ORR was defined as complete (CR) plus partial response (PR). OS was calculated from the date of first immunotherapy administration until death due to any cause. PFS was calculated from the date of first immunotherapy until disease progression or death due to any cause. Comparisons between patient characteristics were performed using Chi-square or Fisher's exact test for discrete variables and the unpaired t test, Wilcoxon sign-rank test or analysis of variance for continuous variables. The best cut-point for total $CD8^+$, $CD103^+$ and $CD103^-$ TIL was assessed using the log-rank maximization method[59]. Survival analyses were performed using the Kaplan-Meier method and the log-rank test. All P-values inferior to 0.05 were considered statistically significant.

A Cox proportional hazards regression model was used to evaluate independent prognostic factors for OS and PFS. Variables included in the final multivariate model were selected according to their clinical relevance and statistical significance in univariate analysis (p-value cut-off = 0.10). The proportional hazard hypothesis was verified with the Schoenfeld residual method. Predictive factors of disease control were tested with logistic regression in univariate and multivariate analyses. The alpha level was 5%. Statistical analyses were performed with R (free software environment for statistical computing and graphics).

Statistical significance was determined with the paired or unpaired Student t-test, or with the one-way analysis of variance (ANOVA) test with Bonferroni correction. Data are presented as mean ± SEM. All statistical details of experiments can be found in Figures and Figure legends; n = number of patient or tumor/lung samples. Statistical analyses were performed with GraphPad Prism software V8 (GraphPad Software Inc., San Diego, CA). * $p<0.05$; ** $p<0.01$; *** $p<0.001$ and RStudio software.

References

1. Tumeh, P.C., Harview, C.L., Yearley, J.H., Shintaku, I.P., Taylor, E.J., Robert, L., Chmielowski, B., Spasic, M., Henry, G., Ciobanu, V., et al. (2014). PD-1 blockade induces responses by inhibiting adaptive immune resistance. Nature 515, 568-571. 2014/11/28.

2. McGranahan, N., Furness, A.J., Rosenthal, R., Ramskov, S., Lyngaa, R., Saini, S.K., Jamal-Hanjani, M., Wilson, G.A., Birkbak, N.J., Hiley, C.T., et al. (2016). Clonal neoantigens elicit T cell immunoreactivity and sensitivity to immune checkpoint blockade. Science (New York), NY 351, 1463-1469.

3. Webb, J.R., Milne, K., Watson, P., Deleeuw, R.J. and Nelson, B.H. (2014). Tumor-infiltrating lymphocytes expressing the tissue resident memory marker CD103 are associated with increased survival in high-grade serous ovarian cancer. Clin Cancer Res 20, 434-444. 2013/11/06.

4. Djenidi, F., Adam, J., Goubar, A., Durgeau, A., Meurice, G., de Montpreville, V., Validire, P., Besse, B. and Mami-Chouaib, F. (2015). CD8+CD103+ tumor-infiltrating lymphocytes are tumor-specific tissue-resident memory T cells and a prognostic factor for survival in lung cancer patients. J Immunol 194, 3475-3486. 2015/03/01.

5. Ganesan, A.P., Clarke, J., Wood, O., Garrido-Martin, E.M., Chee, S.J., Mellows, T., Samaniego-Castruita, D., Singh, D., Seumois, G., Alzetani, A., et al. (2017). Tissue-resident memory features are linked to the magnitude of cytotoxic T cell responses in human lung cancer. Nat Immunol 18, 940-950. 2017/06/20.

6. Nizard, M., Roussel, H., Diniz, M.O., Karaki, S., Tran, T., Voron, T., Dransart, E., Sandoval, F., Riquet, M., Rance, B., et al. (2017). Induction of resident memory T cells enhances the efficacy of cancer vaccine. Nat Commun 8, 15221. 2017/05/26.

7. Savas, P., Virassamy, B., Ye, C., Salim, A., Mintoff, C.P., Caramia, F., Salgado, R., Byrne, D.J., Teo, Z.L., Dushyanthen, S., et al. (2018). Single-cell profiling of breast cancer T cells reveals a tissue-resident memory subset associated with improved prognosis. Nat Med 24, 986-993. 2018/06/27.

8. Clarke, J., Panwar, B., Madrigal, A., Singh, D., Gujar, R., Wood, O., Chee, S.J., Eschweiler, S., King, E.V., Awad, A.S., et al. (2019). Single-cell transcriptomic analysis of tissue-resident memory T cells in human lung cancer. J Exp Med. 2019/06/23.

9. Mackay, L.K., Stock, A.T., Ma, J.Z., Jones, C.M., Kent, S.J., Mueller, S.N., Heath, W.R., Carbone, F.R. and Gebhardt, T. (2012). Long-lived epithelial immunity by tissue-resident memory T (TRM) cells in the absence of persisting local antigen presentation. Proc Natl Acad Sci U S A 109, 7037-7042. 2012/04/18.

10. Hofmann, M. and Pircher, H. (2011). E-cadherin promotes accumulation of a unique memory CD8 T-cell population in murine salivary glands. Proc Natl Acad Sci U S A 108, 16741-16746. 2011/09/21.

11. Ray, S.J., Franki, S.N., Pierce, R.H., Dimitrova, S., Koteliansky, V., Sprague, A.G., Doherty, P.C., de Fougerolles, A.R. and Topham, D.J. (2004). The collagen binding alpha1beta1 integrin VLA-1 regulates CD8 T cell-mediated immune protection against heterologous influenza infection. Immunity 20, 167-179. 2004/02/21.

12. McNamara, H.A., Cai, Y., Wagle, M.V., Sontani, Y., Roots, C.M., Miosge, L.A., O'Connor, J.H., Sutton, H.J., Ganusov, V.V., Heath, W.R., et al. (2017). Up-regulation of LFA-1 allows liver-resident memory T cells to patrol and remain in the hepatic sinusoids. Sci Immunol 2. 2017/07/15.

13. Mackay, L.K., Minnich, M., Kragten, N.A., Liao, Y., Nota, B., Seillet, C., Zaid, A., Man, K., Preston, S., Freestone, D., et al. (2016). Hobit and Blimp1 instruct a universal transcriptional program of tissue residency in lymphocytes. Science 352, 459-463. 2016/04/23.

14. Hombrink, P., Helbig, C., Backer, R.A., Piet, B., Oja, A.E., Stark, R., Brasser, G., Jongejan, A., Jonkers, R.E., Nota, B., et al. (2016). Programs for the persistence, vigilance and control of human CD8(+) lung-resident memory T cells. Nat Immunol 17, 1467-1478. 2016/11/01.

15. Milner, J.J., Toma, C., Yu, B., Zhang, K., Omilusik, K., Phan, A.T., Wang, D., Getzler, A.J., Nguyen, T., Crotty, S., et al. (2017). Runx3 programs CD8(+) T cell residency in non-lymphoid tissues and tumours. Nature 552, 253-257. 2017/12/07.

16. Le Floc'h, A., Jalil, A., Vergnon, I., Le Maux Chansac, B., Lazar, V., Bismuth, G., Chouaib, S. and Mami-Chouaib, F. (2007). Alpha E beta 7 integrin interaction with E-cadherin promotes antitumor CTL activity by triggering lytic granule polarization and exocytosis. J Exp Med 204, 559-570. 2007/02/28.

17. Anikeeva, N., Somersalo, K., Sims, T.N., Thomas, V.K., Dustin, M.L. and Sykulev, Y. (2005). Distinct role of lymphocyte function-associated antigen-1 in mediating effective cytolytic activity by cytotoxic T lymphocytes. Proc Natl Acad Sci U S A 102, 6437-6442. 2005/04/27.

18. Johnston, R.J., Comps-Agrar, L., Hackney, J., Yu, X., Huseni, M., Yang, Y., Park, S., Javinal, V., Chiu, H., Irving, B., et al. (2014). The immunoreceptor TIGIT regulates antitumor and antiviral CD8(+) T cell effector function. Cancer Cell 26, 923-937. 2014/12/04.

19. Guo, X., Zhang, Y., Zheng, L., Zheng, C., Song, J., Zhang, Q., Kang, B., Liu, Z., Jin, L., Xing, R., et al. (2018). Global characterization of T cells in non-small-cell lung cancer by single-cell sequencing. Nat Med 24, 978-985. 2018/06/27.

20. Duhen, T., Duhen, R., Montler, R., Moses, J., Moudgil, T., de Miranda, N.F., Goodall, C.P., Blair, T.C., Fox, B.A., McDermott, J.E., et al. (2018). Co-expression of CD39 and CD103 identifies tumor-reactive CD8 T cells in human solid tumors. Nat Commun 9, 2724. 2018/07/15.

21. Parkhurst, M., Gros, A., Pasetto, A., Prickett, T., Crystal, J.S., Robbins, P. and Rosenberg, S.A. (2017). Isolation of T-Cell Receptors Specifically Reactive with Mutated Tumor-Associated Antigens from Tumor-Infiltrating Lymphocytes Based on CD137 Expression. Clin Cancer Res 23, 2491-2505. 2016/11/09.

22. Gros, A., Robbins, P.F., Yao, X., Li, Y.F., Turcotte, S., Tran, E., Wunderlich, J.R., Mixon, A., Farid, S., Dudley, M.E., et al. (2014). PD-1 identifies the patient-specific CD8(+) tumor-reactive repertoire infiltrating human tumors. J Clin Invest 124, 2246-2259. 2014/03/29.

23. Takada, K., Wang, X., Hart, G.T., Odumade, O.A., Weinreich, M.A., Hogquist, K.A. and Jameson, S.C. (2011). Kruppel-like factor 2 is required for trafficking but not quiescence in postactivated T cells. J Immunol 186, 775-783. 2010/12/17.

24. Skon, C.N., Lee, J.Y., Anderson, K.G., Masopust, D., Hogquist, K.A. and Jameson, S.C. (2013). Transcriptional downregulation of S1pr1 is required for the establishment of resident memory CD8+ T cells. Nat Immunol 14, 1285-1293. 2013/10/29.

25. Cepek, K.L., Shaw, S.K., Parker, C.M., Russell, G.J., Morrow, J.S., Rimm, D.L. and Brenner, M.B. (1994). Adhesion between epithelial cells and T lymphocytes mediated by E-cadherin and the alpha E beta 7 integrin. Nature 372, 190-193. 1994/11/10.

26. Shiow, L.R., Rosen, D.B., Brdickova, N., Xu, Y., An, J., Lanier, L.L., Cyster, J.G. and Matloubian, M. (2006). CD69 acts downstream of interferon-alpha/beta to inhibit S1P1 and lymphocyte egress from lymphoid organs. Nature 440, 540-544. 2006/03/10.

27. Simoni, Y., Becht, E., Fehlings, M., Loh, C.Y., Koo, S.L., Teng, K.W.W., Yeong, J.P.S., Nahar, R., Zhang, T., Kared, H., et al. (2018). Bystander CD8(+) T cells are abundant and phenotypically distinct in human tumour infiltrates. Nature 557, 575-579. 2018/05/18.

28. Scott, A.C., Dundar, F., Zumbo, P., Chandran, S.S., Klebanoff, C.A., Shakiba, M., Trivedi, P., Menocal, L., Appleby, H., Camara, S.J., et al. (2019). TOX is a critical regulator of tumour-specific T cell differentiation. Nature. 2019/06/18.

29. Mackay, L.K., Braun, A., Macleod, B.L., Collins, N., Tebartz, C., Bedoui, S., Carbone, F.R. and Gebhardt, T. (2015). Cutting edge: CD69 interference with sphingosine-1-phosphate receptor function regulates peripheral T cell retention. J Immunol 194, 2059-2063. 2015/01/28.

30. Guan, T., Dominguez, C.X., Amezquita, R.A., Laidlaw, B.J., Cheng, J., Henao-Mejia, J., Williams, A., Flavell, R.A., Lu, J. and Kaech, S.M. (2018). ZEB1, ZEB2, and the miR-200 family form a counterregulatory network to regulate CD8(+) T cell fates. J Exp Med 215, 1153-1168. 2018/02/17.

31. Quintana, F.J., Jin, H., Burns, E.J., Nadeau, M., Yeste, A., Kumar, D., Rangachari, M., Zhu, C., Xiao, S., Seavitt, J., et al. (2012). Aiolos promotes TH17 differentiation by directly silencing Il2 expression. Nat Immunol 13, 770-777. 2012/07/04.

32. Li, H., van der Leun, A.M., Yofe, I., Lubling, Y., Gelbard-Solodkin, D., van Akkooi, A.C.J., van den Braber, M., Rozeman, E.A., Haanen, J., Blank, C.U., et al. (2019). Dysfunctional CD8 T Cells Form a Proliferative, Dynamically Regulated Compartment within Human Melanoma. Cell 176, 775-789 e718. 2019/01/01.

33. Willinger, T., Freeman, T., Herbert, M., Hasegawa, H., McMichael, A.J. and Callan, M.F. (2006). Human naive CD8 T cells down-regulate expression of the WNT pathway transcription factors lymphoid enhancer binding factor 1 and transcription factor 7 (T cell factor-1) following antigen encounter in vitro and in vivo. J Immunol 176, 1439-1446. 2006/01/21.

34. Brummelman, J., Mazza, E.M.C., Alvisi, G., Colombo, F.S., Grilli, A., Mikulak, J., Mavilio, D., Alloisio, M., Ferrari, F., Lopci, E., et al. (2018). High-dimensional single cell analysis identifies stem-like cytotoxic CD8(+) T cells infiltrating human tumors. J Exp Med 215, 2520-2535. 2018/08/30.

35. Im, S.J., Hashimoto, M., Gerner, M.Y., Lee, J., Kissick, H.T., Burger, M.C., Shan, Q., Hale, J.S., Lee, J., Nasti, T.H., et al. (2016). Defining CD8+ T cells that provide the proliferative burst after PD-1 therapy. Nature 537, 417-421. 2016/08/09.

36. Sade-Feldman, M., Yizhak, K., Bjorgaard, S.L., Ray, J.P., de Boer, C.G., Jenkins, R.W., Lieb, D.J., Chen, J.H., Frederick, D.T., Barzily-Rokni, M., et al. (2018). Defining T Cell States Associated with Response to Checkpoint Immunotherapy in Melanoma. Cell 175, 998-1013 e1020. 2018/11/06.

37. Kurtulus, S., Madi, A., Escobar, G., Klapholz, M., Nyman, J., Christian, E., Pawlak, M., Dionne, D., Xia, J., Rozenblatt-Rosen, O., et al. (2019). Checkpoint Blockade Immunotherapy Induces Dynamic Changes in PD-1(-)CD8(+) Tumor-Infiltrating T Cells. Immunity 50, 181-194 e186. 2019/01/13.

38. Miller, B.C., Sen, D.R., Al Abosy, R., Bi, K., Virkud, Y.V., LaFleur, M.W., Yates, K.B., Lako, A., Felt, K., Naik, G.S., et al. (2019). Subsets of exhausted CD8(+) T cells differentially mediate tumor control and respond to checkpoint blockade. Nat Immunol 20, 326-336. 2019/02/20.

39. Siddiqui, I., Schaeuble, K., Chennupati, V., Fuertes Marraco, S.A., Calderon-Copete, S., Pais Ferreira, D., Carmona, S.J., Scarpellino, L., Gfeller, D., Pradervand, S., et al. (2019). Intratumoral Tcf1(+)PD-1(+)CD8(+) T Cells with Stem-like Properties Promote Tumor Control in Response to Vaccination and Checkpoint Blockade Immunotherapy. Immunity 50, 195-211 e110. 2019/01/13.

40. Yost, K.E., Satpathy, A.T., Wells, D.K., Qi, Y., Wang, C., Kageyama, R., McNamara, K.L., Granja, J.M., Sarin, K.Y., Brown, R.A., et al. (2019). Clonal replacement of tumor-specific T cells following PD-1 blockade. Nat Med 25, 1251-1259. 2019/07/31.

41. Mielke, L.A., Liao, Y., Clemens, E.B., Firth, M.A., Duckworth, B., Huang, Q., Almeida, F.F., Chopin, M., Koay, H.F., Bell, C.A., et al. (2019). TCF-1 limits the formation of Tc17 cells via repression of the MAF-RORgammat axis. J Exp Med 216, 1682-1699. 2019/05/31.

42. Cheuk, S., Schlums, H., Gallais Serezal, I., Martini, E., Chiang, S.C., Marquardt, N., Gibbs, A., Detlofsson, E., Introini, A., Forkel, M., et al. (2017). CD49a Expression Defines Tissue-Resident CD8(+) T Cells Poised for Cytotoxic Function in Human Skin. Immunity 46, 287-300. 2017/02/19.

43. Ichiyama, K., Sekiya, T., Inoue, N., Tamiya, T., Kashiwagi, I., Kimura, A., Morita, R., Muto, G., Shichita, T., Takahashi, R., et al. (2011). Transcription factor Smad-independent T helper 17 cell induction by transforming-growth factor-beta is mediated by suppression of eomesodermin. Immunity 34, 741-754. 2011/05/24.

44. Tajima, M., Wakita, D., Satoh, T., Kitamura, H. and Nishimura, T. (2011). IL-17/IFN-gamma double producing CD8+ T (Tc17/IFN-gamma) cells: a novel cytotoxic T-cell subset converted from Tc17 cells by IL-12. Int Immunol 23, 751-759. 2011/11/01.

45. Piet, B., de Bree, G.J., Smids-Dierdorp, B.S., van der Loos, C.M., Remmerswaal, E.B., von der Thusen, J.H., van Haarst, J.M., Eerenberg, J.P., ten Brinke, A., van der Bij, W., et al. (2011). CD8(+) T cells with an intraepithelial phenotype upregulate cytotoxic function upon influenza infection in human lung. J Clin Invest 121, 2254-2263. 2011/05/04.

46. Woodberry, T., Suscovich, T.J., Henry, L.M., August, M., Waring, M.T., Kaur, A., Hess, C., Kutok, J.L., Aster, J.C., Wang, F., et al. (2005). Alpha E beta 7 (CD103) expression identifies

a highly active, tonsil-resident effector-memory CTL population. J Immunol 175, 4355-4362. 2005/09/24.

47. Webb, J.R., Wick, D.A., Nielsen, J.S., Tran, E., Milne, K., McMurtrie, E. and Nelson, B.H. (2010). Profound elevation of CD8+ T cells expressing the intraepithelial lymphocyte marker CD103 (alphaE/beta7 Integrin) in high-grade serous ovarian cancer. Gynecol Oncol 118, 228-236. 2010/06/15.

48. Franciszkiewicz, K., Le Floc'h, A., Jalil, A., Vigant, F., Robert, T., Vergnon, I., Mackiewicz, A., Benihoud, K., Validire, P., Chouaib, S., et al. (2009). Intratumoral induction of CD103 triggers tumor-specific CTL function and CCR5-dependent T-cell retention. Cancer Res 69, 6249-6255. 2009/07/30.

49. Edwards, J., Wilmott, J.S., Madore, J., Gide, T.N., Quek, C., Tasker, A., Ferguson, A., Chen, J., Hewavisenti, R., Hersey, P., et al. (2018). CD103(+) Tumor-Resident CD8(+) T Cells Are Associated with Improved Survival in Immunotherapy-Naive Melanoma Patients and Expand Significantly During Anti-PD-1 Treatment. Clin Cancer Res 24, 3036-3045. 2018/03/31.

50. El-Asady, R., Yuan, R., Liu, K., Wang, D., Gress, R.E., Lucas, P.J., Drachenberg, C.B. and Hadley, G.A. (2005). TGF-{beta}-dependent CD103 expression by CD8(+) T cells promotes selective destruction of the host intestinal epithelium during graft-versus-host disease. J Exp Med 201, 1647-1657. 2005/05/18.

51. Wang, B., Wu, S., Zeng, H., Liu, Z., Dong, W., He, W., Chen, X., Dong, X., Zheng, L., Lin, T., et al. (2015). CD103+ Tumor Infiltrating Lymphocytes Predict a Favorable Prognosis in Urothelial Cell Carcinoma of the Bladder. J Urol 194, 556-562. 2015/03/11.

52. Franciszkiewicz, K., Le Floc'h, A., Boutet, M., Vergnon, I., Schmitt, A. and Mami-Chouaib, F. (2013). CD103 or LFA-1 engagement at the immune synapse between cytotoxic T

cells and tumor cells promotes maturation and regulates T-cell effector functions. Cancer Res 73, 617-628. 2012/11/29.

53. Boutet, M., Gauthier, L., Leclerc, M., Gros, G., de Montpreville, V., Theret, N., Donnadieu, E. and Mami-Chouaib, F. (2016). TGFbeta Signaling Intersects with CD103 Integrin Signaling to Promote T-Lymphocyte Accumulation and Antitumor Activity in the Lung Tumor Microenvironment. Cancer Res 76, 1757-1769. 2016/02/28.

54. Pascutti, M.F., Geerman, S., Collins, N., Brasser, G., Nota, B., Stark, R., Behr, F., Oja, A., Slot, E., Panagioti, E., et al. (2019). Peripheral and systemic antigens elicit an expandable pool of resident memory CD8(+) T cells in the bone marrow. Eur J Immunol. 2019/03/21.

55. Patro, R., Duggal, G., Love, M.I., Irizarry, R.A. and Kingsford, C. (2017). Salmon provides fast and bias-aware quantification of transcript expression. Nat Methods 14, 417-419. 2017/03/07.

56. Pimentel, H., Bray, N.L., Puente, S., Melsted, P. and Pachter, L. (2017). Differential analysis of RNA-seq incorporating quantification uncertainty. Nat Methods 14, 687-690. 2017/06/06.

57. Yu, G., Wang, L.G., Han, Y. and He, Q.Y. (2012). clusterProfiler: an R package for comparing biological themes among gene clusters. OMICS 16, 284-287. 2012/03/30.

58. Bolotin, D.A., Poslavsky, S., Mitrophanov, I., Shugay, M., Mamedov, I.Z., Putintseva, E.V. and Chudakov, D.M. (2015). MiXCR: software for comprehensive adaptive immunity profiling. Nat Methods 12, 380-381. 2015/04/30.

59. Hothorn, TaL., B. (2003). On the Exact Distribution of Maximally Selected Rank Statistics. Computational Statistics & Data Analysis 43, 121-137.

60. Mackay, L.K., Minnich, M., Kragten, N.A., Liao, Y., Nota, B., Seillet, C., Zaid, A., Man, K., Preston, S., Freestone, D., et al. (2016). Hobit and Blimp1 instruct a universal transcriptional program of tissue residency in lymphocytes. Science 352, 459-463. 2016/04/23.

61. Johnston, R.J., Comps-Agrar, L., Hackney, J., Yu, X., Huseni, M., Yang, Y., Park, S., Javinal, V., Chiu, H., Irving, B., et al. (2014). The immunoreceptor TIGIT regulates antitumor and antiviral CD8(+) T cell effector function. Cancer Cell 26, 923-937. 2014/12/04.

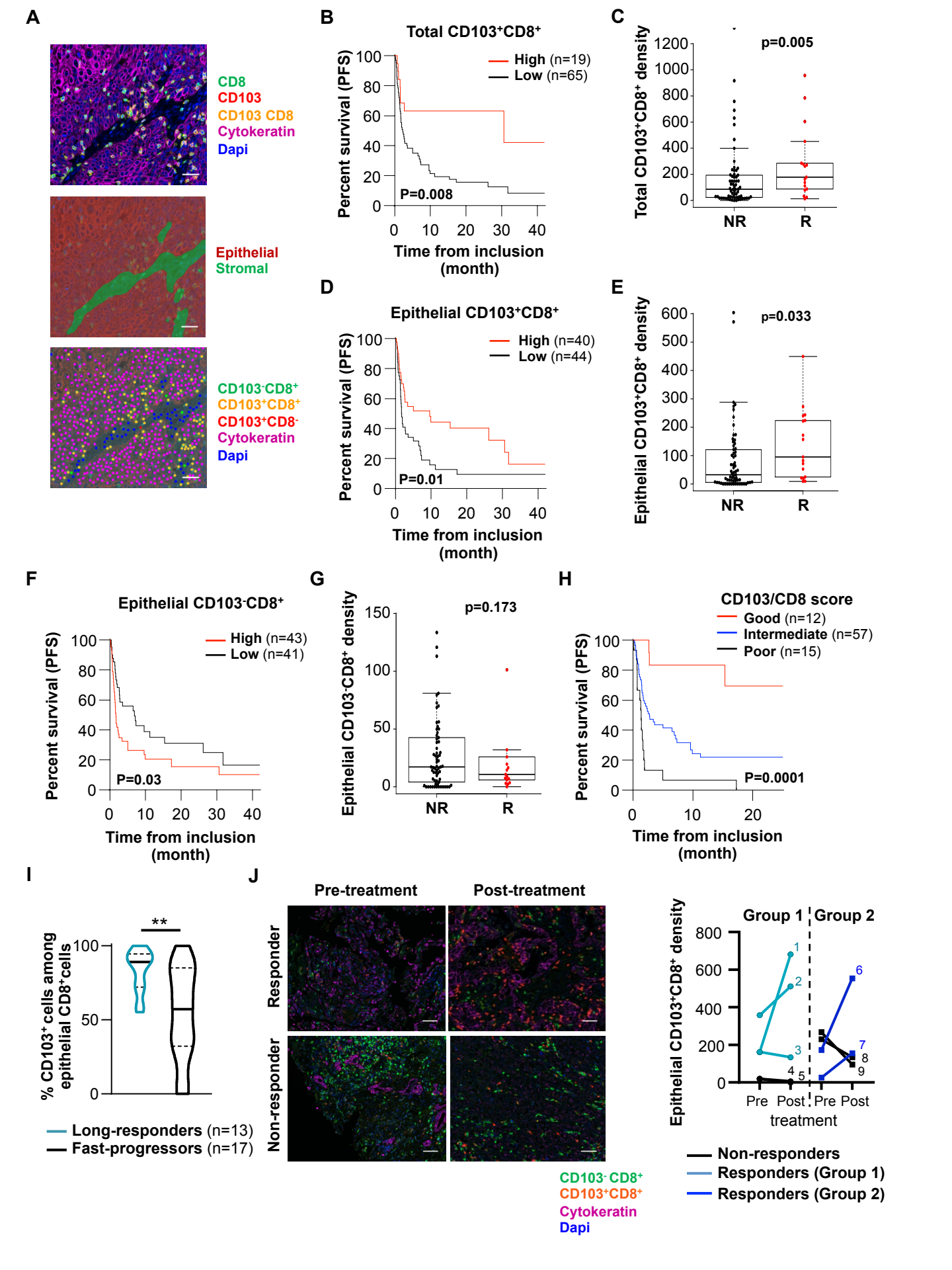
A
CD8
CD103
CD103 CD8
Cytokeratin
Dapi
Epithelial
Stromal
CD103-CD8+
CD103+CD8+
CD103+CD8-
Cytokeratin
Dapi
B
Total CD103+CD8+
High (n=19)
Low (n=65)
Percent survival (PFS)
P=0.008
Time from inclusion (month)
C
Total CD103+CD8+ density
p=0.005
NR
R
D
Epithelial CD103+CD8+
High (n=40)
Low (n=44)
Percent survival (PFS)
P=0.01
Time from inclusion (month)
E
Epithelial CD103+CD8+ density
p=0.033
NR
R
F
Epithelial CD103-CD8+
High (n=43)
Low (n=41)
Percent survival (PFS)
P=0.03
Time from inclusion (month)
G
Epithelial CD103-CD8+ density
p=0.173
NR
R
H
CD103/CD8 score
Good (n=12)
Intermediate (n=57)
Poor (n=15)
Percent survival (PFS)
P=0.0001
Time from inclusion (month)
I
% CD103+ cells among epithelial CD8+cells
**
Long-responders (n=13)
Fast-progressors (n=17)
J
Pre-treatment
Post-treatment
Responder
Non-responder
CD103- CD8+
CD103+CD8+
Cytokeratin
Dapi
Group 1
Group 2
Epithelial CD103+CD8+ density
Pre
Post
Pre
Post
treatment
Non-responders
Responders (Group 1)
Responders (Group 2)

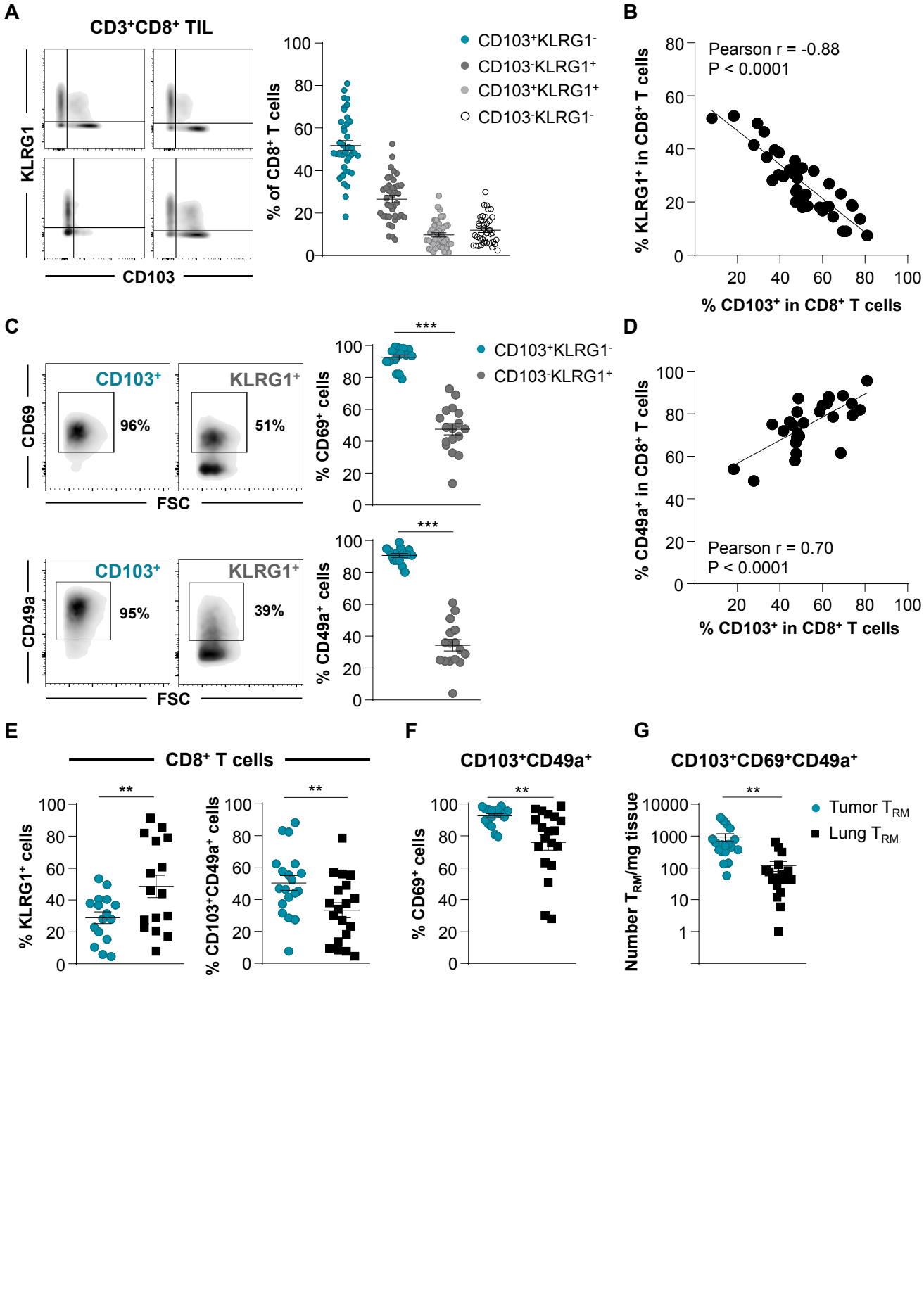
A
CD3+CD8+ TIL
KLRG1
CD103
% of CD8+ T cells
CD103+KLRG1-
CD103-KLRG1+
CD103+KLRG1+
CD103-KLRG1-
B
Pearson r = -0.88
P < 0.0001
% KLRG1+ in CD8+ T cells
% CD103+ in CD8+ T cells
C
CD103+
KLRG1+
96%
51%
CD69
FSC
% CD69+ cells
***
CD103+KLRG1-
CD103-KLRG1+
95%
39%
CD49a
% CD49a+ cells
D
Pearson r = 0.70
P < 0.0001
% CD49a+ in CD8+ T cells
% CD103+ in CD8+ T cells
E
CD8+ T cells
% KLRG1+ cells
% CD103+CD49a+ cells
**
F
CD103+CD49a+
% CD69+ cells
G
CD103+CD69+CD49a+
Number TRM/mg tissue
Tumor TRM
Lung TRM

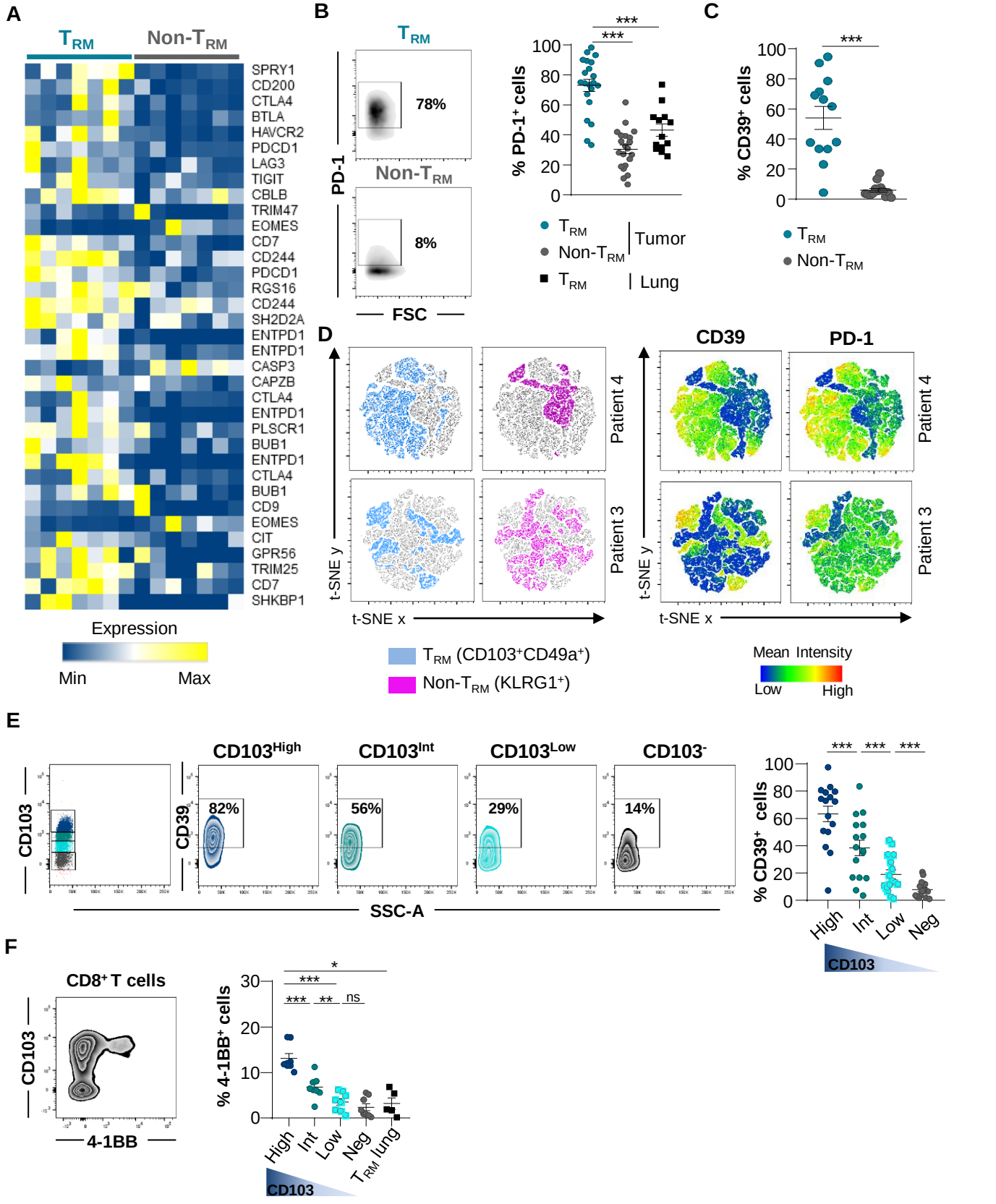
A
TRM
Non-TRM
SPRY1
CD200
CTLA4
BTLA
HAVCR2
PDCD1
LAG3
TIGIT
CBLB
TRIM47
EOMES
CD7
CD244
PDCD1
RGS16
CD244
SH2D2A
ENTPD1
ENTPD1
CASP3
CAPZB
CTLA4
ENTPD1
PLSCR1
BUB1
ENTPD1
CTLA4
BUB1
CD9
EOMES
CIT
GPR56
TRIM25
CD7
SHKBP1
Expression
Min
Max
B
TRM
78%
Non-TRM
8%
PD-1
FSC
% PD-1+ cells
***
***
TRM
Non-TRM
Tumor
TRM
Lung
C
% CD39+ cells
***
TRM
Non-TRM
D
CD39
PD-1
Patient 4
Patient 3
t-SNE y
t-SNE x
TRM (CD103+CD49a+)
Non-TRM (KLRG1+)
Mean Intensity
Low
High
E
CD103High
CD103Int
CD103Low
CD103-
CD103
CD39
82%
56%
29%
14%
SSC-A
% CD39+ cells
***
***
***
High
Int
Low
Neg
CD103
F
CD8+ T cells
CD103
4-1BB
% 4-1BB+ cells
*
***
***
**
ns
High
Int
Low
Neg
TRM lung
CD103

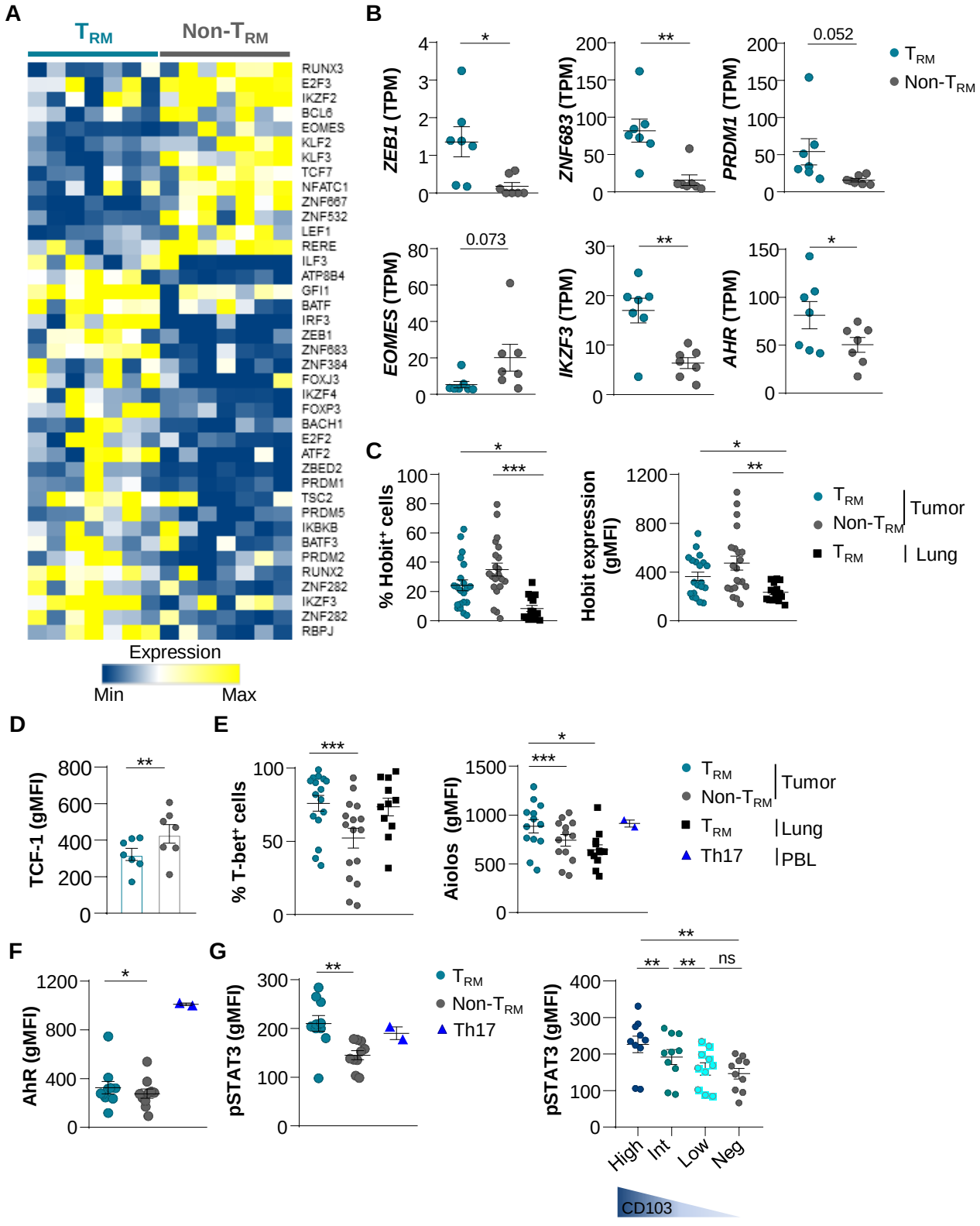
A
TRM
Non-TRM
RUNX3
E2F3
IKZF2
BCL6
EOMES
KLF2
KLF3
TCF7
NFATC1
ZNF667
ZNF532
LEF1
RERE
ILF3
ATP8B4
GFI1
BATF
IRF3
ZEB1
ZNF683
ZNF384
FOXJ3
IKZF4
FOXP3
BACH1
E2F2
ATF2
ZBED2
PRDM1
TSC2
PRDM5
IKBKB
BATF3
PRDM2
RUNX2
ZNF282
IKZF3
ZNF282
RBPJ
Expression
Min
Max
B
ZEB1 (TPM)
ZNF683 (TPM)
PRDM1 (TPM)
0.052
EOMES (TPM)
0.073
IKZF3 (TPM)
AHR (TPM)
TRM
Non-TRM
C
% Hobit+ cells
Hobit expression (gMFI)
TRM
Non-TRM
Tumor
TRM
Lung
D
TCF-1 (gMFI)
E
% T-bet+ cells
Aiolos (gMFI)
TRM
Non-TRM
Tumor
TRM
Lung
Th17
PBL
F
AhR (gMFI)
G
pSTAT3 (gMFI)
TRM
Non-TRM
Th17
pSTAT3 (gMFI)
ns
High
Int
Low
Neg
CD103

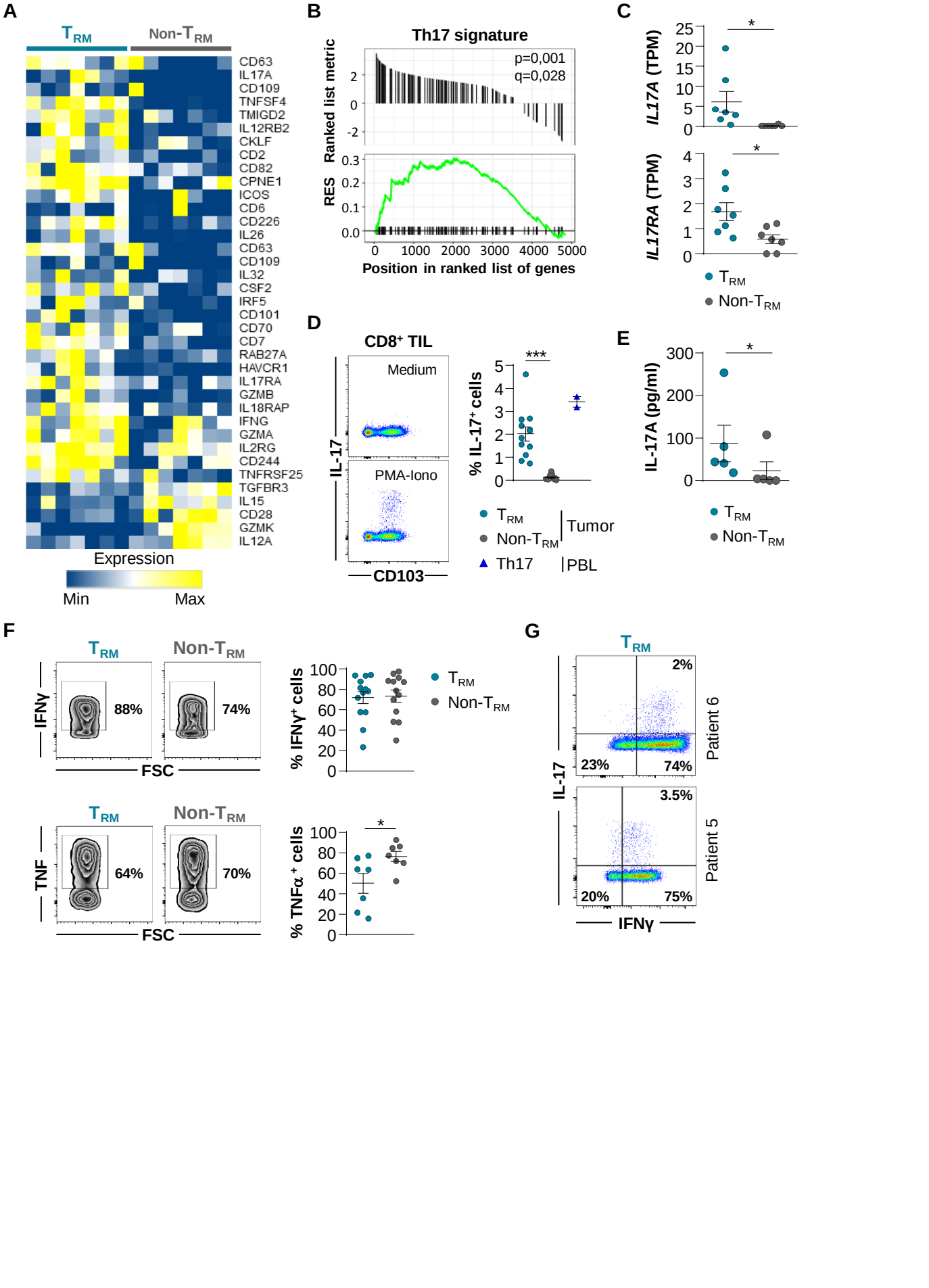
A
TRM
Non-TRM
CD63
IL17A
CD109
TNFSF4
TMIGD2
IL12RB2
CKLF
CD2
CD82
CPNE1
ICOS
CD6
CD226
IL26
CD63
CD109
IL32
CSF2
IRF5
CD101
CD70
CD7
RAB27A
HAVCR1
IL17RA
GZMB
IL18RAP
IFNG
GZMA
IL2RG
CD244
TNFRSF25
TGFBR3
IL15
CD28
GZMK
IL12A
Expression
Min
Max
B
Th17 signature
p=0,001
q=0,028
Ranked list metric
RES
Position in ranked list of genes
C
IL17A (TPM)
IL17RA (TPM)
TRM
Non-TRM
D
CD8+ TIL
Medium
PMA-Iono
IL-17
CD103
% IL-17+ cells
TRM
Non-TRM
Th17
Tumor
PBL
E
IL-17A (pg/ml)
TRM
Non-TRM
F
TRM
Non-TRM
IFNγ
88%
74%
FSC
% IFNγ+ cells
TNF
64%
70%
% TNFα+ cells
G
TRM
2%
23%
74%
Patient 6
3.5%
20%
75%
Patient 5
IL-17
IFNγ

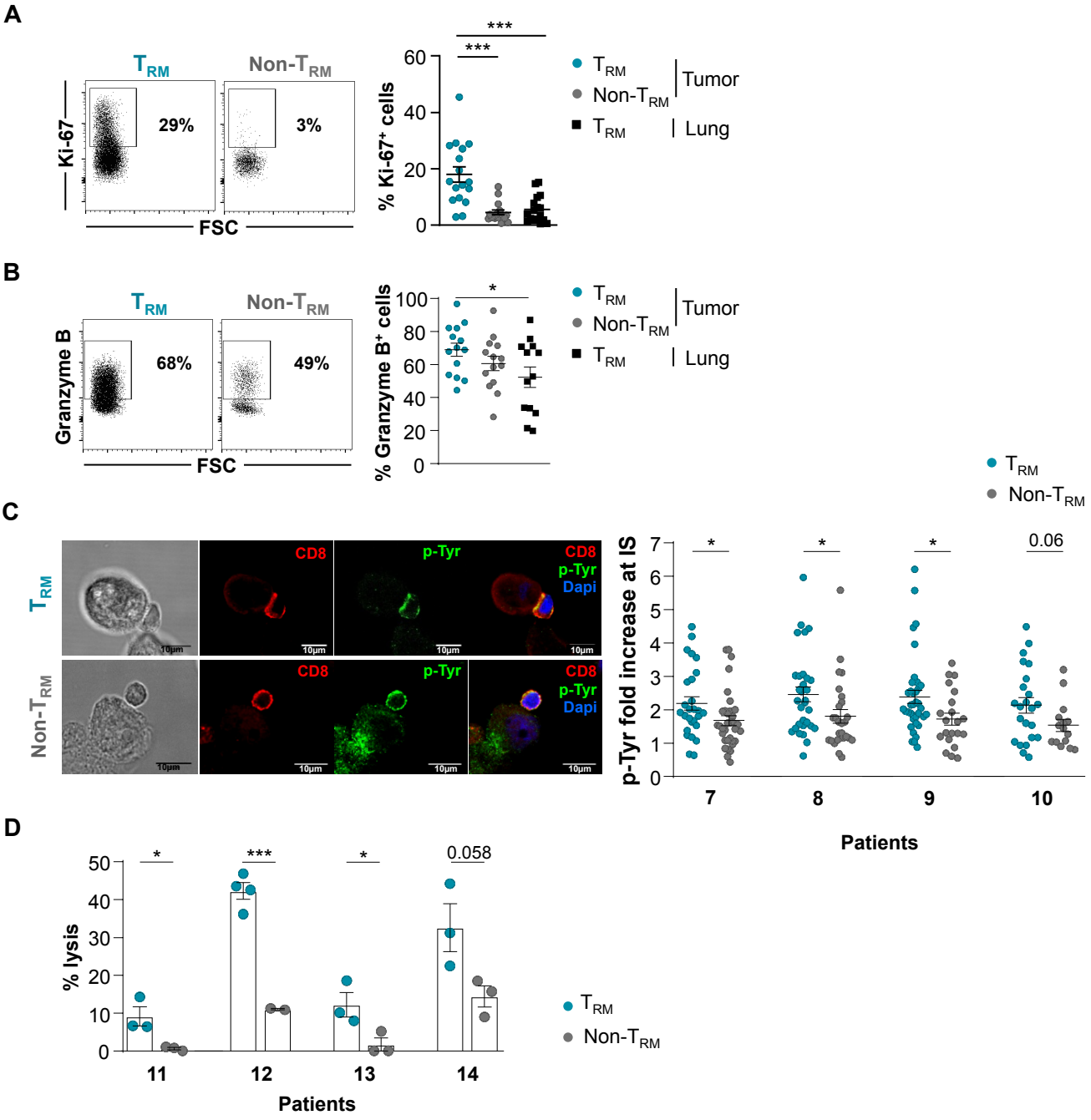
A
TRM
Non-TRM
Ki-67
29%
3%
FSC
% Ki-67+ cells
***
***
TRM
Non-TRM
Tumor
TRM
Lung
B
TRM
Non-TRM
Granzyme B
68%
49%
FSC
% Granzyme B+ cells
*
TRM
Non-TRM
Tumor
TRM
Lung
C
TRM
Non-TRM
CD8
p-Tyr
CD8
p-Tyr
Dapi
10µm
p-Tyr fold increase at IS
*
*
*
0.06
7
8
9
10
Patients
TRM
Non-TRM
D
% lysis
*
***
*
0.058
11
12
13
14
Patients
TRM
Non-TRM

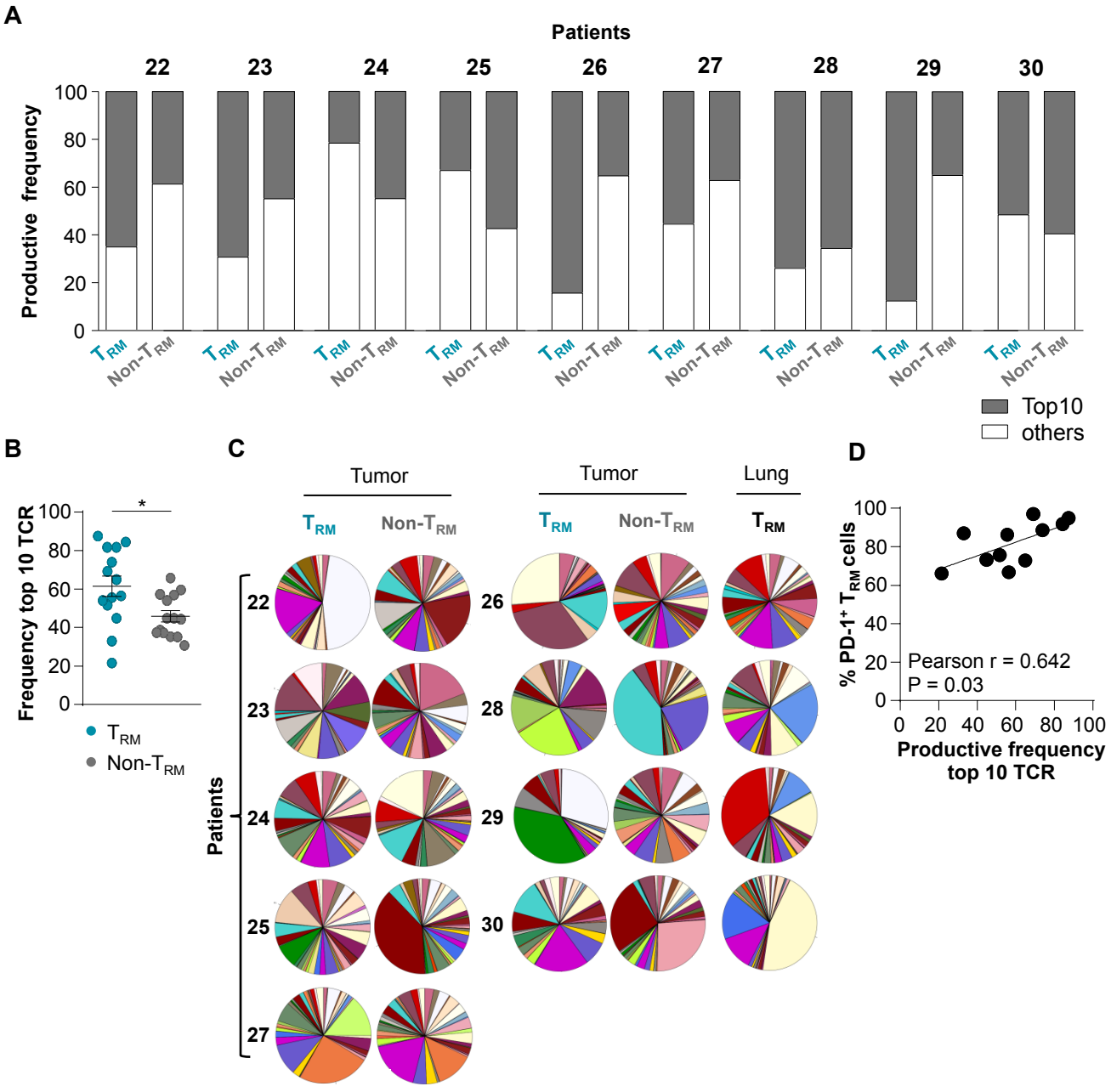
A
Patients
22
23
24
25
26
27
28
29
30
Productive frequency
100
80
60
40
20
0
TRM
Non-TRM
Top10
others
B
Frequency top 10 TCR
*
TRM
Non-TRM
C
Tumor
Tumor
Lung
TRM
Non-TRM
TRM
Non-TRM
TRM
Patients
22
23
24
25
27
26
28
29
30
D
% PD-1+ TRM cells
Pearson r = 0.642
P = 0.03
Productive frequency
top 10 TCR

eTOC blurb

Using retrospective cohorts of anti-PD-(L)1-treated NSCLC, Corgnac et al. show that the density of $CD103^+CD8^+$ cells in tumors is associated with better progression-free survival. $CD103^+CD8^+$ tumor-infiltrating lymphocytes are specific resident memory T cells (T_{RM}) enriched in a subset with unique Tc1/Tc17 differentiation program that differs from $CD103^-CD8^+$ T cells (non-T_{RM}).

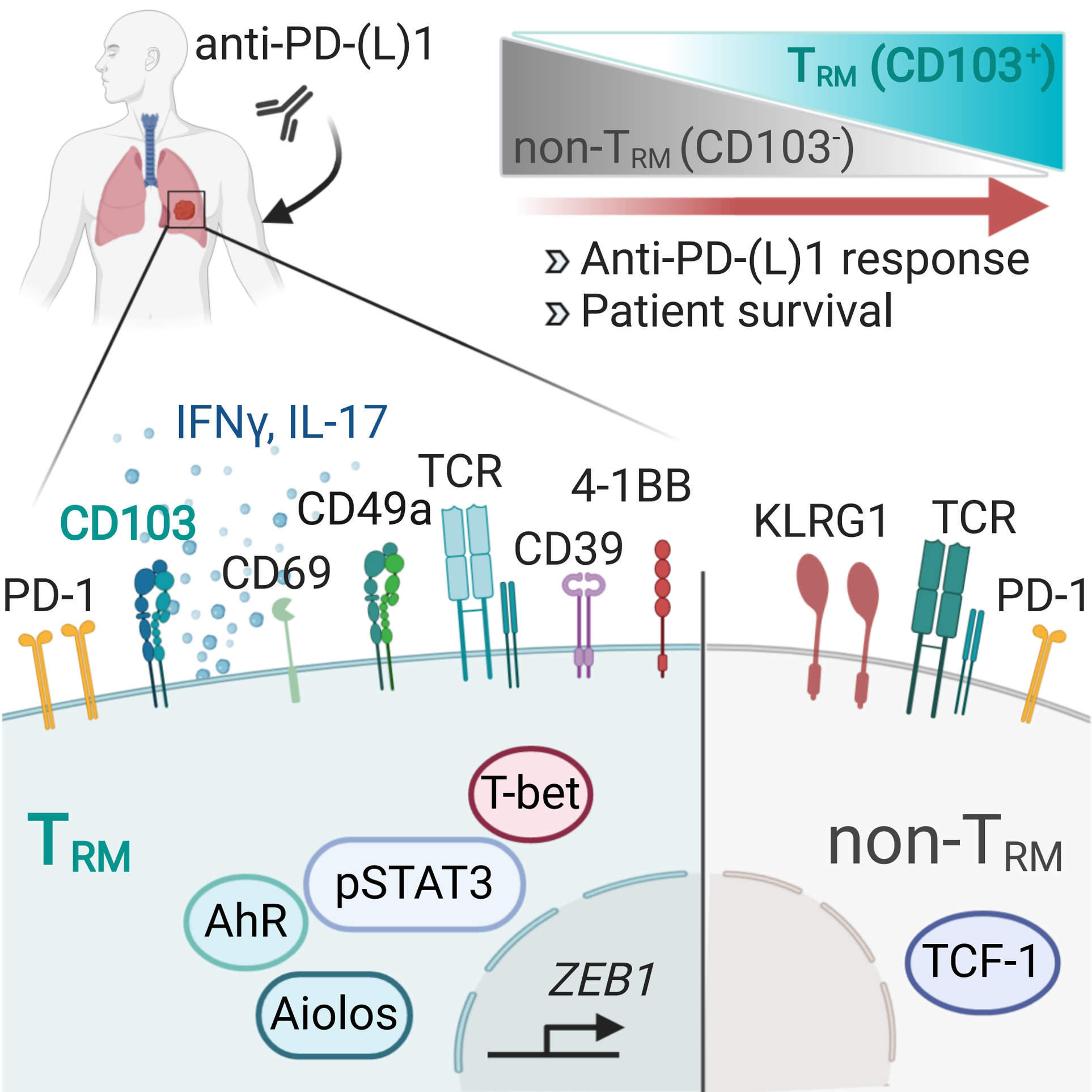
anti-PD-(L)1
T_{RM} ($CD103^+$)
non-T_{RM} ($CD103^-$)
Anti-PD-(L)1 response
Patient survival
IFNγ, IL-17
CD103
CD49a
TCR
4-1BB
CD69
CD39
PD-1
KLRG1
TCR
PD-1
T_{RM}
T-bet
pSTAT3
AhR
Aiolos
ZEB1
non-T_{RM}
TCF-1